NAVAL POSTGRADUATE SCHOOL
MONTEREY, CALIFORNIA

THESIS

RECOVERY FACTORS IN ZERO-MEAN INTERNAL OSCILLATORY FLOWS

by

Nicole Lynn Tait

December 1995

Thesis Advisor: Ashok Gopinath
Thesis Co-Advisor: Oscar Biblarz

Approved for public release; distribution is unlimited.

REPORT DOCUMENTATION PAGE

Form Approved OMB No. 0704-0188

1. AGENCY USE ONLY *(Leave blank)*	2. REPORT DATE December 1995	3. REPORT TYPE AND DATES COVERED Master's Thesis

4. TITLE AND SUBTITLE RECOVERY FACTORS IN ZERO-MEAN INTERNAL OSCILLATORY FLOWS

5. FUNDING NUMBERS

6. AUTHOR(S) Nicole Lynn Tait

7. PERFORMING ORGANIZATION NAME(S) AND ADDRESS(ES)
Naval Postgraduate School
Monterey CA 93943-5000

8. PERFORMING ORGANIZATION REPORT NUMBER

9. SPONSORING/MONITORING AGENCY NAME(S) AND ADDRESS(ES)

10. SPONSORING/MONITORING AGENCY REPORT NUMBER

11. SUPPLEMENTARY NOTES The views expressed in this thesis are those of the author and do not reflect the official policy or position of the Department of Defense or the U.S. Government.

12a. DISTRIBUTION/AVAILABILITY STATEMENT
Approved for public release; distribution is unlimited.

12b. DISTRIBUTION CODE

13. ABSTRACT *(maximum 200 words)*

High speed oscillatory flows, like high speed mean flows, are capable of inducing time-averaged heat transfer effects. This research involves the analytical solution of a model problem of zero-mean internal oscillatory flow, which arises from a high-intensity resonant standing acoustic wave set up across the ends of two parallel plates. The compressible form of the Navier-Stokes equations are solved, along with the equations of continuity, energy, and state, using perturbation solution and complex variable methods. MAPLE, a symbolic mathematical software tool, is utilized to find the time-averaged portion of the temperature distribution between the plates. The final heat transfer results are presented in terms of suitably defined recovery factors. The analysis is performed for varying gap widths between the plates using air as the host fluid. This work provides the fundamental explanation of the phenomenon responsible for the thermoacoustic refrigerating effect as well as an analytical basis for determining the optimum gap width between the plates of the stack in a thermoacoustic refrigerator.

14. SUBJECT TERMS recovery factor, oscillatory flow, heat transfer, thermoacoustic refrigeration			15. NUMBER OF PAGES 76
			16. PRICE CODE
17. SECURITY CLASSIFICATION OF REPORT Unclassified	18. SECURITY CLASSIFICATION OF THIS PAGE Unclassified	19. SECURITY CLASSIFICATION OF ABSTRACT Unclassified	20. LIMITATION OF ABSTRACT UL

NSN 7540-01-280-5500

Standard Form 298 (Rev. 2-89)
Prescribed by ANSI Std. 239-18 298-102

Approved for public release; distribution is unlimited.

RECOVERY FACTORS IN ZERO-MEAN INTERNAL OSCILLATORY FLOWS

Nicole Lynn Tait
Lieutenant, United States Naval Reserve
B.S., University of Maryland, 1989

Submitted in partial fulfillment
of the requirements for the degrees of

MASTER OF SCIENCE IN MECHANICAL ENGINEERING
MASTER OF SCIENCE IN ASTRONAUTICAL ENGINEERING

from the
NAVAL POSTGRADUATE SCHOOL
December 1995

Author: Nicole Lynn Tait
Nicole Lynn Tait

Approved by:
Ashok Gopinath, Thesis Advisor

Oscar Biblarz, Thesis Co-Advisor

M. D. Kelleher, Chairman, Department of Mechanical Engineering

D.J. Collins, Chairman, Department of Aeronautical and Astronautical Engineering

ABSTRACT

High speed oscillatory flows, like high speed mean flows, are capable of inducing time-averaged heat transfer effects. This research involves the analytical solution of a model problem of zero-mean internal oscillatory flow, which arises from a high-intensity resonant standing acoustic wave set up across the ends of two parallel plates. The compressible form of the Navier-Stokes equations are solved, along with the equations of continuity, energy, and state, using perturbation solution and complex variable methods. MAPLE, a symbolic mathematical software tool, is utilized to find the time-averaged portion of the temperature distribution between the plates. The final heat transfer results are presented in terms of suitably defined recovery factors. The analysis is performed for varying gap widths between the plates using air as the host fluid. This work provides the fundamental explanation of the phenomenon responsible for the thermoacoustic refrigerating effect as well as an analytical basis for determining the optimum gap width between the plates of the stack in a thermoacoustic refrigerator.

TABLE OF CONTENTS

LIST OF FIGURES

LIST OF SYMBOLS, ACRONYMS AND/OR ABBREVIATIONS

α	thermal diffusivity, m^2/s
β	coefficient of thermal expansion, K^{-1}
c	speed of sound, m/s
c_p	specific heat at constant pressure, J/kg K
c_v	specific heat at constant volume, J/kg K
δ	boundary layer thickness, m
δ_α	thermal penetration depth, m
δ_v	viscous penetration depth or Stokes's boundary layer thickness, m
Ec	Eckert number
ϕ	dimensionless temperature
γ	ratio of specific heats
h	convection heat transfer coefficient, W/m^2 K
η_0	gap width parameter
k	acoustic wave number, m^{-1}
k_c	thermal conductivity, W/m K
λ	acoustic wavelength, m
M	Mach number
μ	dynamic viscosity, kg/s m
Nu	Nusselt number
ν	kinematic viscosity, m^2/s
p	pressure, N/m^2
p_m	mean pressure, N/m^2
Pr	Prandtl number
q'''	imposed heat generation, W/m^3
q_w	heat flux at the wall, W/m^2
r	recovery factor
R	gas constant, J/kg K
ρ	mass density, kg/m^3
ρ_m	mean density, kg/m^3
t	time, s
T	temperature, K
T_m	mean temperature, K
ΔT_{ref}	reference temperature, K
u	velocity in x-direction, m/s
v	velocity in y-direction, m/s
V_0	velocity amplitude in x-direction, m/s
w	velocity in z-direction, m/s
ω	acoustic frequency, radians
y_0	gap half-width, m

I. INTRODUCTION

This research involves the study of the time-averaged heat transfer effects induced by high speed internal zero-mean oscillatory flows. The model problem being treated is for an ideal-gas host fluid between two "infinite", parallel plates. The zero-mean oscillatory flow is produced by a high-intensity standing axial acoustic wave induced across the ends of the plates. The plates are separated by a distance, $2y_0$, and the sound wave has a wavenumber of $k=2\pi/\lambda$ where λ is the wavelength. The relationship between these two parameters, y_0 and k, is assumed to be such that $y_0k<<1$ throughout the analysis. In other words, the narrow acoustic waveguide approximation, which is discussed further in Chapter III, holds true for this research. Another general assumption made for this analysis is that the host fluid between the plates is a gas which is treated as ideal.

The particular focus of this study is to solve analytically the Navier-Stokes equations for this problem. The governing equations are set up and simplified using the particular geometry and assumptions pertinent to this particular case. Then, the variables are scaled in a standard fashion to reduce the equations of continuity, momentum, energy and state into dimensionless forms. An order of magnitude analysis is performed to further simplify the equations. Finally, perturbation methods are employed, and like-order terms are grouped to form new equations. The equations of most significant order are solved analytically using complex variable methods for their respective unknowns. The final goal is to determine the resulting time-averaged temperature distribution and study its affects on the heat transfer behavior at the walls. MAPLE, a symbolic computational software package (see Blachman and Mossinghoff (1994)), is utilized to

perform the extensive mathematical manipulations that are required in this analysis. The results of the time-averaged thermal behavior that is ultimately of interest are presented, by convention, in terms of suitably defined recovery factors.

The entire analysis is performed for two separate cases, which differ based on the width of separation between the plates, $2y_0$, in comparison with a length scale called the Stokes's boundary layer thickness, δ_v. The Stokes's boundary layer thickness, also called the viscous penetration depth, is defined in Schlichting (1979) in the discussion of Stokes's second problem concerning the flow near an oscillating plate as the thickness of the layer of fluid which is carried by the plate. If the quantity, y_0/δ_v, is greater than or equal to a certain amount (which is determined in this research and discussed in Chapter IV), the spacing between the plates is considered to be a "wide gap." The first and simpler case is analyzed using a wide gap geometry and its respective assumptions. In the second case, an arbitrary gap width is considered which lifts some simplifying assumptions so that it includes "narrow gaps." The arbitrary gap case is useful for analysis of the time-averaged transport behavior in the stack region of a thermoacoustic refrigerator.

II. BACKGROUND

Since the time-averaged heat transfer results of this work are presented in terms of conventionally defined recovery factors, it is useful to review the concept of a recovery factor. In order to do so, the application of recovery factors to two well studied flows, namely Couette and Poiseuille flows, will be presented here as adapted from Burmeister (1983).

Couette flow, as illustrated in Figure 2.1, occurs when fluid exists between two infinite parallel plates.

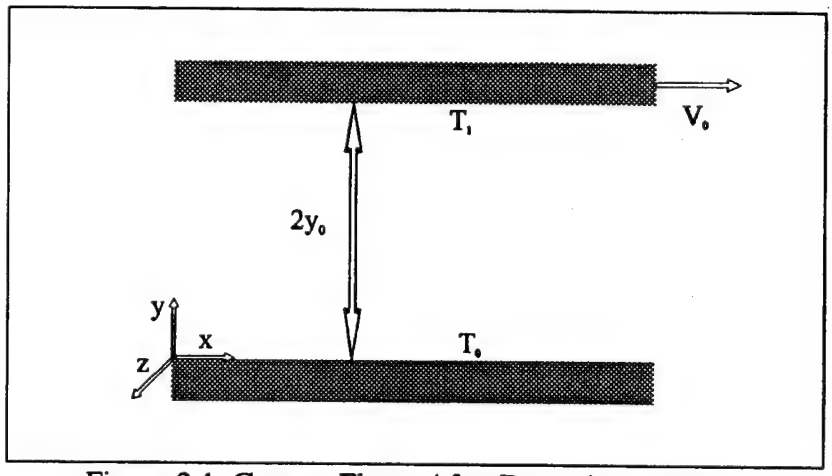

Figure 2.1 Couette Flow. After Burmeister (1983).

One plate (the upper plate here) is moving with a velocity V_0, and the other (lower) plate is stationary. The plates are at different temperatures, T_0 and T_1. If both plates were stationary, the temperature distribution between them would simply be linear; however, the fluid motion caused by the motion of the upper plate affects the temperature distribution. This effect comes from viscous dissipation and is especially significant in high speed flows. Applying the following assumptions and boundary conditions to the

governing equations of continuity, momentum, and energy, the velocity and temperature distributions are determined.

The assumptions being made are: (1) steady conditions, (2) laminar flow, (3) constant properties, (4) no pressure gradient in the x direction, (5) no edge effects or end effects, (6) Newtonian fluid, and (7) no buoyancy or other body forces.

Boundary Conditions:	At y=0:	u=0=w	(no slip at wall)
		v=0	(no penetration at wall)
		T=T_0	(fixed wall temperature)
	At y=2y_0:	u=V_0, w=0	(no slip at wall)
		v=0	(no penetration at wall)
		T=T_1	(fixed wall temperature)

The resulting velocity distribution is linear as given below:

$$\frac{u}{V_0} = \frac{y}{2y_0} \tag{2.1}$$

The resulting temperature distribution is given by

$$\frac{T - T_0}{T_1 - T_0} = \frac{y}{2y_0} + (Ec\,\mathrm{Pr})(\frac{y}{2y_0})(1 - \frac{y}{2y_0}) \tag{2.2}$$

where $Ec = \dfrac{V_0^2}{2c_p(T_1 - T_0)}$, which represents a comparison of viscous dissipation effects to the imposed temperature difference, and $\mathrm{Pr} = \dfrac{\mu c_p}{k_c}$ is the Prandtl number of the fluid.

Using Fourier's law, the heat flux at the lower plate is given by

$$q_w = -k_c \left.\frac{dT}{dy}\right|_{y=0} = -k_c \frac{T_1 - T_0}{2y_0}(1 + Ec\,\mathrm{Pr}) = \frac{k_c[T_0 - (T_1 + \dfrac{\mathrm{Pr}\,V_0^2}{2c_p})]}{2y_0} \tag{2.3}$$

Therefore, the heat transfer is not actually driven by the simple difference in temperature, T_0-T_1. Instead, there is a contribution from the kinetic energy of the fluid being converted into thermal energy at the lower plate through viscous dissipation. If the same Couette flow were analyzed with an adiabatic boundary condition at the lower plate ($\frac{\partial T}{\partial y} = 0$ at y=0), the resulting temperature distribution would be

$$T - T_1 = \frac{\Pr V_0^2}{2c_p}\left(\frac{1 - y^2}{(2y_0)^2}\right) \tag{2.4}$$

The corresponding temperature at the lower plate is called the "adiabatic wall temperature" and is given by

$$T_{aw} = T(y = 0) = T_1 + \frac{\Pr V_0^2}{2c_p} \tag{2.5}$$

Thus, using Fourier's law from Equation 2.3, it is seen that the heat transfer at the wall can be expressed as

$$q_w = \frac{k_c(T_{wall} - T_{aw})}{2y_0} \tag{2.6}$$

where T_{wall}=T_0 from before. Now it is observed that the heat transfer is driven solely by the temperature difference, T_{wall}-T_{aw}, where T_{aw} is not constant but varies depending on the particular geometry and flow conditions being studied.

This result incorporates, into a simple form, the effects of viscous dissipation on heat transfer which become more and more significant as V_0 and the kinetic energy of the fluid increase. It also allows the heat transfer coefficient to be expressed in a more consistent and convenient manner as

$$h = \frac{q_w}{(T_{wall} - T_{aw})} = \frac{k_c}{2y_0} \tag{2.7}$$

The heat transfer coefficient, as a result, is never negative; and the Nusselt number, $Nu = \frac{2hy_0}{k_c}$, conveniently has the value of one.

From the expression for the adiabatic wall temperature in Equation 2.5, it is clearly observed that some of the fluid's kinetic energy, $\frac{V_0^2}{2}$, is being converted into thermal energy. In a sense, some of this kinetic energy is being "recovered" as thermal energy at the lower adiabatic wall which then results in a rise in temperature of that wall. The ratio of the thermal energy recovered at an adiabatic surface to the kinetic energy of the fluid is called the recovery factor, *r*. For this Couette flow, the recovery factor is

$$r = \frac{c_p(T_{aw} - T_1)}{\frac{V_0^2}{2}} = \Pr \tag{2.8}$$

The physical significance of the recovery factor, as a measure of viscous dissipation effects, applies equally well for other types of flow and wall conditions, even for situations with *non-adiabatic* surfaces. For any situation, "*r*" contains information about how much of the fluid's kinetic energy is converted into thermal energy at the walls. It is defined and calculated, however, in a similar manner to that of the Couette flow example - the ratio of the recovered thermal energy at an *adiabatic* surface to the fluid's kinetic energy. The expression of the kinetic energy may differ depending on the velocity chosen to base it on, but the temperature difference used for calculation is always

T_{aw}-T_{wall}. Of course, for other types of flow, the resulting expression for the recovery factor may be more complicated than simply a linear Prandtl number dependence.

Another type of flow is Poiseuille flow which is of direct relevance to the current work. In Poiseuille flow, pictured in Figure 2.2, both surfaces are stationary. The assumptions applied to this case are the same as for the Couette flow case with the exception that there is a uniform pressure gradient in the x direction which drives a uni-directional mean flow. Using the following boundary conditions, the velocity and temperature distributions are determined.

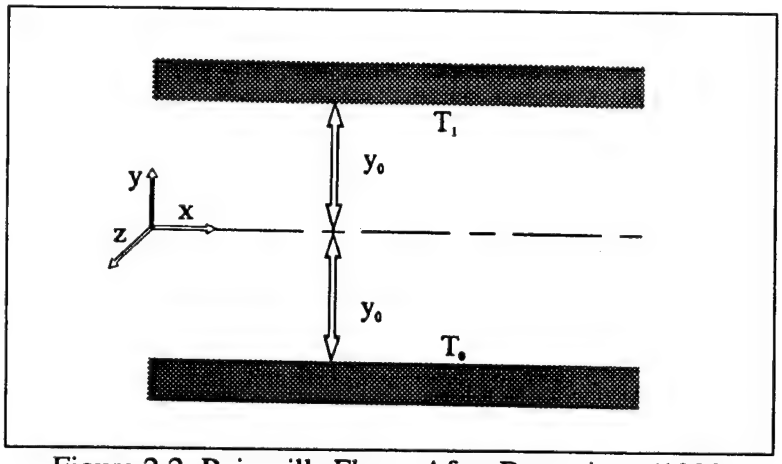

Figure 2.2 Poiseuille Flow. After Burmeister (1983).

Boundary Conditions:	At $y=-y_0$:	$u=0=w$	(no slip at wall)
		v=0	(no penetration at wall)
		$T=T_0$	(fixed wall temperature)
	At $y=+y_0$:	$u=0=w$	(no slip at wall)
		v=0	(no penetration at wall)
		$T=T_1$	(fixed wall temperature)

The resulting velocity distribution is given by

$$u = \frac{y_0^2}{2\mu}\left(-\frac{dp}{dx}\right)\left(1-\frac{y^2}{y_0^2}\right) \tag{2.9}$$

The definition of average velocity,

$$u_{av} = \frac{1}{2y_0}\int_{-y_0}^{y_0} u dy, \tag{2.10}$$

gives

$$u_{av} = \frac{y_0^2}{3}(-\frac{dp}{dx}) \tag{2.11}$$

Also the maximum velocity, which occurs at the centerline (y=0) is given by

$$u_m = \frac{y_0^2}{2}(-\frac{dp}{dx}) = \frac{3}{2}u_{av} \tag{2.12}$$

The velocity distribution from Equation 2.9 may then be expressed in terms of either the average or the maximum velocity as

$$u = u_m(1-\frac{y^2}{y_0^2}) \quad \text{or} \quad u = \frac{3}{2}u_{av}(1-\frac{y^2}{y_0^2}) \tag{2.13}$$

The resulting temperature distribution for this Poiseuille flow is given by

$$T = T_0 + \frac{T_1 - T_0}{2}(1+\frac{y}{y_0}) + \frac{\mu}{3k_c}u_m^2(1-\frac{y^4}{y_0^4}) \tag{2.14}$$

From Fourier's law, the wall heat flux at the lower wall is given by

$$q_w = -k_c\frac{dT}{dy}(y=-y_0) = \frac{k_c[T_0 - (T_1 + \frac{6\,\mathrm{Pr}\,u_{av}^2}{c_p})]}{2y_0} \tag{2.15}$$

Using the concepts established in the Couette flow case, the adiabatic wall temperature for Poiseuille flow is deduced to be

$$T_{aw} = T_1 + \frac{6\,\mathrm{Pr}\,u_{av}^2}{c_p} \tag{2.16}$$

This can be also easily verified by solving the adiabatic wall case and finding the temperature of the adiabatic wall.

Again, it is observed that the driving potential for heat transfer between the walls is the difference in temperature, T_{wall}-T_{aw}. This ensures that viscous dissipation effects are accounted for and that the heat transfer coefficient, $h = \frac{k_c}{2y_0}$, is always positive. The Nusselt number, $Nu = \frac{2hy_0}{k_c}$, is again unity. The recovery factor, r, is then given by

$$r = \frac{c_p(T_{aw} - T_1)}{\frac{u_{av}^2}{2}} = 12\,\mathrm{Pr} \tag{2.17}$$

Note that the kinetic energy of the fluid was chosen to be represented in terms of the average velocity.

These concepts of an adiabatic wall temperature and a corresponding recovery factor apply to other geometries and flow conditions and are typically of consequence in high speed flows where velocity gradients and viscous dissipation effects are significant. In high speed mean flows, a sufficient amount of the fluid's kinetic energy is transformed into thermal energy, causing significant heat transfer to occur at the walls from viscous dissipation. Normally, the result is a heating of the walls.

Recovery factors will be found for the geometry and flow conditions present in this research which are similar to the example case of Poiseuille flow just considered. The physical geometry is exactly the same with the presence of two parallel plates. The principal difference in the current problem is in the flow conditions. In this case a driving (zero-mean) oscillatory pressure gradient is set up across the plates by a high-intensity

resonant standing acoustic wave. This contrasts to the uni-directional mean flow which occurs in Poiseuille flow. Despite being a zero-mean oscillatory flow, the cross-coupling between the harmonics is capable of inducing a time-averaged flow and a thermal effect which can be significant in high speed situations. This key idea introduces a number of interesting new features into the problem which are explored in this research. The posed problem and its solution will be addressed further in Chapter III, and the corresponding recovery factor will be discussed extensively in Chapter IV.

III. THEORY

A. THE MODEL PROBLEM AND GOVERNING EQUATIONS

The model problem consists of high speed oscillatory flow between two "infinite" parallel plates and is depicted in Figure 3.1. Both plates are held at a fixed temperature, T_m. The host fluid, air, oscillates between the plates in the x^* direction with a velocity amplitude of oscillation, V_0, and a frequency, ω, in radians.

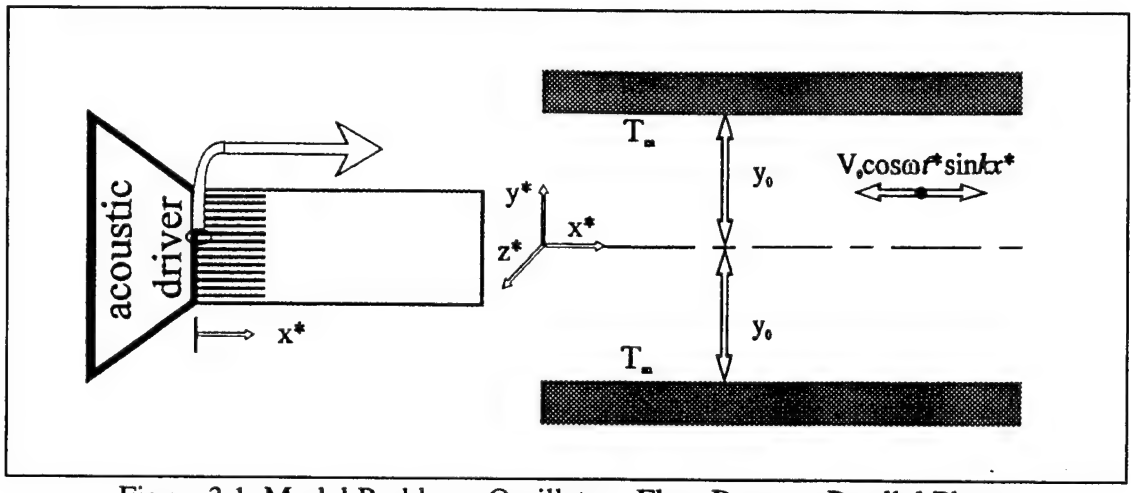

Figure 3.1 Model Problem: Oscillatory Flow Between Parallel Plates.

This flow is induced by a high intensity standing acoustic wave set up across the ends of the plates. The acoustic wave number is $k=2\pi/\lambda$ where λ is the acoustic wavelength. The wavelengths of concern in this research are on the order of 1 meter. The distance between the plates is $2y_0$, and a Cartesian coordinate system is established with the origin at the centerline. Using a wavelength of the above mentioned order, 1 meter, the narrow acoustic waveguide approximation, $y_0k<<1$, requires that y_0 be much less than 1 meter. In this research, the gap widths ($2y_0$) studied are on the order of

millimeters or tenths of millimeters. Therefore, the narrow acoustic waveguide approximation certainly holds throughout this work.

To determine the temperature distribution between the plates, which is the fundamental objective of this study, the compressible form of the equations of continuity, motion, and energy are solved analytically. These equations in Cartesian coordinates are (asterisks (*) denote a dimensional quantity):

Continuity: $$\frac{\partial \rho^*}{\partial t^*} + \frac{\partial}{\partial x^*}(\rho^* u^*) + \frac{\partial}{\partial y^*}(\rho^* v^*) + \frac{\partial}{\partial z^*}(\rho^* w^*) = 0 \tag{3.1}$$

Motion:

x * component:

$$\rho^*\left(\frac{\partial u^*}{\partial t^*} + u^*\frac{\partial u^*}{\partial x^*} + v^*\frac{\partial u^*}{\partial y^*} + w^*\frac{\partial u^*}{\partial z}\right) = \rho^* g_x^* - \frac{\partial p^*}{\partial x^*} + \frac{\partial}{\partial x^*}\left[\mu\left(2\frac{\partial u^*}{\partial x^*} - \frac{2}{3}\left(\frac{\partial u^*}{\partial x^*} + \frac{\partial v^*}{\partial y^*} + \frac{\partial w^*}{\partial z^*}\right)\right)\right] + \frac{\partial}{\partial y^*}\left[\mu\left(\frac{\partial u^*}{\partial y^*} + \frac{\partial v^*}{\partial x^*}\right)\right] + \frac{\partial}{\partial z^*}\left[\mu\left(\frac{\partial w^*}{\partial x^*} + \frac{\partial u^*}{\partial z^*}\right)\right] \tag{3.2a}$$

y * component:

$$\rho^*\left(\frac{\partial v^*}{\partial t^*} + u^*\frac{\partial v^*}{\partial x^*} + v^*\frac{\partial v^*}{\partial y^*} + w^*\frac{\partial v^*}{\partial z}\right) = \rho^* g_y^* - \frac{\partial p^*}{\partial y^*} + \frac{\partial}{\partial y^*}\left[\mu\left(2\frac{\partial v^*}{\partial y^*} - \frac{2}{3}\left(\frac{\partial u^*}{\partial x^*} + \frac{\partial v^*}{\partial y^*} + \frac{\partial w^*}{\partial z^*}\right)\right)\right] + \frac{\partial}{\partial z^*}\left[\mu\left(\frac{\partial v^*}{\partial z^*} + \frac{\partial w^*}{\partial y^*}\right)\right] + \frac{\partial}{\partial x^*}\left[\mu\left(\frac{\partial u^*}{\partial y^*} + \frac{\partial v^*}{\partial x^*}\right)\right] \tag{3.2b}$$

z * component:

$$\rho^*\left(\frac{\partial w^*}{\partial t^*} + u^*\frac{\partial w^*}{\partial x^*} + v^*\frac{\partial w^*}{\partial y^*} + w^*\frac{\partial w^*}{\partial z}\right) = \rho^* g_z^* - \frac{\partial p^*}{\partial z^*} + \frac{\partial}{\partial z^*}\left[\mu\left(2\frac{\partial w^*}{\partial z^*} - \frac{2}{3}\left(\frac{\partial u^*}{\partial x^*} + \frac{\partial v^*}{\partial y^*} + \frac{\partial w^*}{\partial z^*}\right)\right)\right] + \frac{\partial}{\partial x^*}\left[\mu\left(\frac{\partial w^*}{\partial x^*} + \frac{\partial u^*}{\partial z^*}\right)\right] + \frac{\partial}{\partial y^*}\left[\mu\left(\frac{\partial v^*}{\partial z^*} + \frac{\partial w^*}{\partial y^*}\right)\right] \tag{3.2c}$$

Energy:

$$\rho^* C_p\left(\frac{\partial T^*}{\partial t^*} + u^*\frac{\partial T^*}{\partial x^*} + v^*\frac{\partial T^*}{\partial y^*} + w^*\frac{\partial T^*}{\partial z}\right) = \left\{\frac{\partial}{\partial x^*}\left(k_c\frac{\partial T^*}{\partial x^*}\right) + \frac{\partial}{\partial y^*}\left(k_c\frac{\partial T^*}{\partial y^*}\right) + \frac{\partial}{\partial z^*}\left(k_c\frac{\partial T^*}{\partial z^*}\right)\right\} + q''' + \beta T^*\left(\frac{\partial p^*}{\partial t^*} + u^*\frac{\partial p^*}{\partial x^*} + v^*\frac{\partial p^*}{\partial y^*} + w^*\frac{\partial p^*}{\partial z}\right) + \mu\Phi^* \tag{3.3a}$$

where:

$$\Phi^* = 2\left[\left(\frac{\partial u^*}{\partial x^*}\right)^2 + \left(\frac{\partial v^*}{\partial y^*}\right)^2 + \left(\frac{\partial w^*}{\partial z^*}\right)^2\right] + \left[\frac{\partial v^*}{\partial x^*} + \frac{\partial u^*}{\partial y^*}\right]^2 + \left[\frac{\partial w^*}{\partial y^*} + \frac{\partial v^*}{\partial z^*}\right]^2 + \left[\frac{\partial u^*}{\partial z^*} + \frac{\partial w^*}{\partial x^*}\right]^2 - \frac{2}{3}\left[\frac{\partial u^*}{\partial x^*} + \frac{\partial v^*}{\partial y^*} + \frac{\partial w^*}{\partial z^*}\right]^2 \tag{3.3b}$$

Note that in the energy equation, β denotes the coefficient of thermal expansion, and Φ^* is called the viscous dissipation function.

Certain basic assumptions being applied to this problem are: (1) narrow acoustic waveguide approximation, $y_0 k \ll 1$, (2) no spanwise (z^*) dependence and no edge effects, $\frac{\partial}{\partial z^*} = 0$, (3) no gravitational field effects, $g_x^* = g_y^* = g_z^* = 0$, (4) no imposed heat generation, $q''' = 0$, and (5) fluid is a gas which may be treated as being ideal with constant properties (dynamic viscosity, μ, specific heat at constant pressure, c_p, and thermal conductivity, k_c). The following boundary conditions are also imposed:

At $y^* = \pm y_0$: $u^* = 0$ (no slip at wall)

$v^* = 0$ (no penetration at wall)

$T^* = T_m$ (fixed wall temperature, called mean temperature)

At $y^* = 0$: $\frac{\partial u^*}{\partial y^*} = 0$ (symmetry)

$v^* = 0$ ("zero-crossover")

The governing equations are transformed into dimensionless equations by scaling the dimensional variables using the standard scales for the flow fluctuation quantities in an acoustic field. The scaling relations are:

$$t = \omega t^*, \quad x = \frac{x^*}{(\lambda / 2\pi)} = kx^*, \quad y = \frac{y^*}{y_0}, \quad u = \frac{u^*}{V_0}, \quad \mathrm{v} = \frac{\mathrm{v}^*}{(V_0 y_0 k)} \tag{3.4}$$

$$\rho = \frac{(\rho^* - \rho_m)}{(\rho_m M)}, \quad p = \frac{p^* - p_m}{(\rho_m V_0 c)}, \quad \phi = \frac{T^* - T_m}{\Delta T_{ref}}, \tag{3.5}$$

where the Mach number is $M = \frac{V_0}{c}$, c is the speed of sound, ρ_m is the mean mass density, p_m is the mean pressure, and the reference temperature, ΔT_{ref}, is as yet undefined.

After implementing the scaling factors, applying the assumptions, and utilizing algebraic manipulations in order to simplify the expressions, the terms with order of magnitude of $y_0^2 k^2 << 1$ are neglected. The resulting dimensionless equations are:

Continuity: $$\frac{\partial \rho}{\partial t} + M\frac{\partial}{\partial x}(\rho u) + \frac{\partial u}{\partial x} + M\frac{\partial}{\partial y}(\rho \mathrm{v}) + \frac{\partial \mathrm{v}}{\partial y} = 0 \tag{3.6}$$

x - Momentum:

$$(\rho M + 1)\left(\frac{\partial u}{\partial t} + Mu\frac{\partial u}{\partial x} + M\mathrm{v}\frac{\partial u}{\partial y}\right) = -\frac{\partial p}{\partial x} + \left(\frac{\delta^2}{y_0^2}\right)\frac{\partial^2 u}{\partial y^2} \tag{3.7}$$

where the boundary layer thickness is $\delta = \frac{\delta_\nu}{\sqrt{2}} = \sqrt{\frac{\nu}{\omega}}$, and the kinematic viscosity is $\nu = \frac{\mu}{\rho_m}$.

y - Momentum:

$$(\rho M+1)(\frac{\partial \mathrm{v}}{\partial t}+Mu\frac{\partial \mathrm{v}}{\partial x}+M\mathrm{v}\frac{\partial \mathrm{v}}{\partial y})=-(\frac{1}{y_0^2k^2})\frac{\partial p}{\partial y}+(\frac{\delta^2}{y_0^2})\frac{\partial^2 \mathrm{v}}{\partial y^2} \tag{3.8}$$
$$+(\frac{\lambda_B}{\mu}+\frac{1}{3})(\frac{\delta^2}{y_0^2})(\frac{\partial^2 u}{\partial y\partial x}+\frac{\partial^2 \mathrm{v}}{\partial y^2})$$

Energy:

$$(\rho M+1)(\frac{\partial \phi}{\partial t}+Mu\frac{\partial \phi}{\partial x}+M\mathrm{v}\frac{\partial \phi}{\partial y})=(\frac{\delta^2}{y_0^2}\frac{1}{\mathrm{Pr}})\frac{\partial^2 \phi}{\partial y^2}+ \tag{3.9}$$
$$2\beta Ec(\phi\Delta T_{ref}+T_m)[(\frac{1}{M})\frac{\partial p}{\partial t}+u\frac{\partial p}{\partial x}+\mathrm{v}\frac{\partial p}{\partial y}]+2Ec(\frac{\delta^2}{y_0^2})(\frac{\partial u}{\partial y})^2$$

where the Eckert number is $Ec=\dfrac{\Delta T_{ref}}{(V_0^2/2c_p)}$, and the Prandtl number is $\mathrm{Pr}=\dfrac{\nu}{\alpha}$ where α is the thermal diffusivity.

B. SOLUTION PROCEDURE

Using order of magnitude analysis and $y_0^2k^2 \ll 1$, the pressure gradient term is the only dominant term in the y-momentum equation (Equation 3.8) which, therefore, reduces to $\dfrac{\partial p}{\partial y}\approx 0$. This allows the boundary layer approximation to be made that pressure is dependent only on x and t ($p \equiv p(x,t)$).

The remaining governing equations are solved utilizing a regular perturbation analysis. The perturbation method assumes a solution of the form:

$$f=f_1+\varepsilon f_2+\varepsilon^2 f_3+\ldots \tag{3.10}$$

where ε is a small quantity. In this problem, the appropriate small quantity, the perturbation parameter, is the Mach number, M. Therefore, solutions are chosen in the forms:

$$\begin{aligned} u &= u_1 + Mu_2 + M^2 u_3 + \dots \\ \phi &= \frac{1}{M}\phi_0 + \phi_1 + M\phi_2 + M^2\phi_3 + \dots \\ \rho &= \rho_1 + M\rho_2 + M^2\rho_3 + \dots \\ v &= v_1 + Mv_2 + M^2 v_3 + \dots \\ p &= p_1 + Mp_2 + M^2 p_3 + \dots \end{aligned} \tag{3.11}$$

Note that the ϕ solution includes a term of order M^{-1} (written $O(M^{-1})$), since a term of that order appears in the energy equation (Equation 3.9).

These solution forms in Equation 3.11 are substituted back into Equations 3.6, 3.7, 3.8 and 3.9 which are subsequently expanded algebraically and ordered according to the powers of M. The like order terms are grouped, and separate sets of partial differential equations are extracted for each order. The most significant solutions are those with orders M^{-1} and M^0 (or O(1)), with the remaining higher order effects not being considered in this study.

Overall, the dimensionless equations to be solved are

Continuity: O(1): $$\frac{\partial \rho_1}{\partial t} + \frac{\partial u_1}{\partial x} + \frac{\partial v_1}{\partial y} = 0 \tag{3.12}$$

x - Momentum: O(1): $$\frac{\partial u_1}{\partial t} = -\frac{\partial p_1}{\partial x} + \left(\frac{1}{2\eta_0^2}\right)\frac{\partial^2 u_1}{\partial y^2} \tag{3.13}$$

where $\eta_0 = \frac{y_0}{\delta_\nu}$ is a gap width parameter based on the viscous penetration depth, $\delta_\nu = \sqrt{\frac{2\nu}{\omega}}$.

Energy: $O(M^{-1})$:
$$\frac{\partial \phi_0}{\partial t} = \frac{1}{2\eta_0^2 \,\mathrm{Pr}} \frac{\partial^2 \phi_0}{\partial y^2} + 2\beta T_m Ec\left(1 + \frac{\phi_1 \Delta T_{ref}}{T_m}\right)\frac{\partial p_1}{\partial t} \tag{3.14}$$

Energy: O(1):
$$\begin{aligned}\frac{\partial \phi_1}{\partial t} + \rho_1 \frac{\partial \phi_0}{\partial t} + u_1 \frac{\partial \phi_0}{\partial x} + \nu_1 \frac{\partial \phi_0}{\partial y} &= \frac{1}{2\eta_0^2 \,\mathrm{Pr}} \frac{\partial^2 \phi_1}{\partial y^2} + 2\beta T_m Ec \frac{\Delta T_{ref}}{T_m}\left(\phi_0 \frac{\partial p_3}{\partial t}\right. \\ &+ \phi_1 \frac{\partial p_2}{\partial t} + \phi_2 \frac{\partial p_1}{\partial t} + \phi_0 u_1 \frac{\partial p_2}{\partial x} + \phi_0 u_2 \frac{\partial p_1}{\partial x} + \phi_1 u_1 \frac{\partial p_1}{\partial x}\Big) + 2\beta T_m Ec \frac{\partial p_2}{\partial t} \\ &+ 2\beta T_m Ec u_1 \frac{\partial p_1}{\partial x} + \frac{Ec}{\eta_0^2}\left(\frac{\partial u_1}{\partial y}\right)^2\end{aligned} \tag{3.15}$$

The variables, u, ϕ, ρ, ν, and p are real functions of time as well as spatial variables. In general, a real variable, Z, can be expressed as the real part of a complex function as follows:

$$Z(x,y,t) = \mathrm{Re}[\bar{z}(x,y)e^{\mathrm{int}}] = \frac{1}{2}[\bar{z}e^{\mathrm{int}} + \bar{z}^{**}e^{-\mathrm{int}}] \tag{3.16}$$

where $\bar{z}(x,y)$ is the complex amplitude, $\bar{z}^{**}$ is the complex conjugate of $\bar{z}(x,y)$, and "n" represents the n^{th} harmonic. Applying this concept to the unknown variables in Equations 3.12, 3.13, 3.14, and 3.15, it follows that:

$$
\begin{aligned}
u_1(x,y,t) &= \mathrm{Re}[\bar{u}_1(x,y)e^{it}] = \frac{1}{2}[\bar{u}_1 e^{it} + \bar{u}_1 **e^{-it}] \\
\phi_0(x,y,t) &= \mathrm{Re}[\bar{\phi}_0(x,y)e^{it}] = \frac{1}{2}[\bar{\phi}_0 e^{it} + \bar{\phi}_0 **e^{-it}] \\
\phi_1(x,y,t) &= \phi_{10}(x,y) + \mathrm{Re}[\bar{\phi}_{12}(x,y)e^{2it}] = \phi_{10}(x,y) + \frac{1}{2}[\bar{\phi}_{12} e^{2it} + \bar{\phi}_{12} **e^{-2it}] \\
\rho_1(x,y,t) &= \mathrm{Re}[\bar{\rho}_1(x,y)e^{it}] = \frac{1}{2}[\bar{\rho}_1 e^{it} + \bar{\rho}_1 **e^{-it}] \\
v_1(x,y,t) &= \mathrm{Re}[\bar{v}_1(x,y)e^{it}] = \frac{1}{2}[\bar{v}_1 e^{it} + \bar{v}_1 **e^{-it}] \\
p_1(x,t) &= \mathrm{Re}[\bar{p}_1(x)e^{it}] = \frac{1}{2}[\bar{p}_1 e^{it} + \bar{p}_1 **e^{-it}]
\end{aligned}
\tag{3.17}
$$

The variables, u_1, ϕ_0, ρ_1, v_1, and p_1 exhibit leading order behavior, whereas ϕ_1, u_2, ρ_2, and all others contribute to higher order behavior. These two categories of behavior are analyzed in turn in the following sections. The behavior of the pressure distribution, however, is particularly significant to this work; therefore, the analysis of p_1 is treated in a separate section following the discussion of the other leading order terms.

C. LEADING ORDER BEHAVIOR

The leading order equations to be solved are as follows:

Continuity: O(1): $$\frac{\partial \rho_1}{\partial t} + \frac{\partial u_1}{\partial x} + \frac{\partial v_1}{\partial y} = 0 \tag{3.18}$$

x - Momentum: O(1): $$\frac{\partial u_1}{\partial t} = -\frac{\partial p_1}{\partial x} + \left(\frac{1}{2\eta_0^2}\right)\frac{\partial^2 u_1}{\partial y^2} \tag{3.19}$$

Energy: O(M^{-1}): $$\frac{\partial \phi_0}{\partial t} = \frac{1}{2\eta_0^2 \,\mathrm{Pr}}\frac{\partial^2 \phi_0}{\partial y^2} + 2\beta T_m Ec\left(1 + \frac{\phi_1 \Delta T_{ref}}{T_m}\right)\frac{\partial p_1}{\partial t} \tag{3.20}$$

The reference temperature is defined to be $\Delta T_{ref} \equiv \frac{V_0^2}{2c_p}$. Using the fact that $c^2 = \gamma R T_m$ (where $\gamma = \frac{c_p}{c_v}$ is the ratio of specific heats, and $R = c_p - c_v$ is the difference of specific heats), the equality, $\frac{\Delta T_{ref}}{T_m} = M^2(\frac{\gamma - 1}{2})$, can be shown. Applying this equality to Equation 3.20 and subsequently neglecting terms of order M^2, Equation 3.20 further reduces to:

Energy: $O(M^{-1})$: $$\frac{\partial \phi_0}{\partial t} = \frac{1}{2\eta_0^2 \Pr}\frac{\partial^2 \phi_0}{\partial y^2} + 2\beta T_m Ec \frac{\partial p_1}{\partial t} \tag{3.21}$$

Substituting the relations from Equation 3.17 into Equations 3.18, 3.19, and 3.21 yields the following complex partial differential equations for the first harmonic quantities:

Continuity: $$\frac{\partial \bar{v}_1}{\partial y} = -i\bar{\rho}_1 - \frac{\partial \bar{u}_1}{\partial x} \tag{3.22}$$

x - Momentum: $$\frac{\partial^2 \bar{u}_1}{\partial y^2} - 2\eta_0^2 i\bar{u}_1 = 2\eta_0^2 \frac{d\bar{p}_1}{dx} \tag{3.23}$$

Energy: $O(M^{-1})$: $$\frac{\partial^2 \bar{\phi}_0}{\partial y^2} - 2\eta_0^2 \Pr i\bar{\phi}_0 = -4\eta_0^2 \Pr Ec\beta_m T_m \bar{p}_1(x) \tag{3.24}$$

The leading order equations to be solved are now Equations 3.22, 3.23, and 3.24. Using the imposed boundary conditions along with the proper equation of state, $\bar{u}_1, \bar{\phi}_0, \bar{\rho}_1, \bar{v}_1$, and $\bar{p}_1$ are found.

The equation of state gives density as a function of pressure and temperature, $\rho=\rho(p,T)$. A differential element, $\Delta\rho^*$, is then given as

$$\Delta\rho^* = \left(\frac{\partial \rho^*}{\partial p^*}\right)_{T^*} \Delta p^* + \left(\frac{\partial \rho^*}{\partial T^*}\right)_{p^*} \Delta T^* \tag{3.25}$$

Now,

$$\left(\frac{\partial \rho^*}{\partial p^*}\right)_{T^*} = \frac{\gamma}{c^2}, \quad \Delta p^* = p^* - p_m = p\rho_m V_0 c \tag{3.26}$$

Also,

$$\Delta T^* = T^* - T_m = \phi \Delta T_{ref} \quad \text{and} \quad \Delta\rho^* = \rho^* - \rho_m = \rho\rho_m M \tag{3.27}$$

From the definition of the coefficient of thermal expansion, $\beta = -\frac{1}{\rho^*}\left(\frac{\partial \rho^*}{\partial T^*}\right)_{p^*}$, it follows that:

$$\left(\frac{\partial \rho^*}{\partial T^*}\right)_{p^*} = -\beta\rho^* = -\beta\rho_m(1 + M\rho) \tag{3.28}$$

Utilizing all of these relations, Equation 3.25 becomes

$$\rho\rho_m M = \frac{\gamma}{c^2} p\rho_m V_0 c - \beta_m \rho_m (1 + M\rho)\phi \Delta T_{ref} \tag{3.29}$$

Substituting in the perturbation solution forms from Equation 3.11, the following equation results for ρ_1:

$$\rho_1 = \gamma p_1 - \beta_m T_m (\gamma - 1)\phi_0 \tag{3.30}$$

Using the complex notation established in Equation 3.17, it results that:

$$\bar{\rho}_1 = \gamma \bar{p}_1 - \beta_m T_m (\gamma - 1)\bar{\phi}_0 \tag{3.31}$$

For ease of following this discussion, the final leading order equations to be solved and their corresponding boundary conditions are summarized below:

Continuity: $$\frac{\partial \bar{v}_1}{\partial y} = -i\bar{\rho}_1 - \frac{\partial \bar{u}_1}{\partial x} \tag{3.32}$$

x - Momentum: $$\frac{\partial^2 \bar{u}_1}{\partial y^2} - 2\eta_0^2 i\bar{u}_1 = 2\eta_0^2 \frac{d\bar{p}_1}{dx} \tag{3.33}$$

Energy: $O(M^{-1})$: $$\frac{\partial^2 \bar{\phi}_0}{\partial y^2} - 2\eta_0^2 \,\mathrm{Pr}\, i\bar{\phi}_0 = -4\eta_0^2 \,\mathrm{Pr}\, Ec\beta_m T_m \bar{p}_1(x) \tag{3.34}$$

Equation of state: $$\bar{\rho}_1 = \gamma\bar{p}_1 - \beta_m T_m(\gamma - 1)\bar{\phi}_0 \tag{3.35}$$

Boundary Conditions:

At $y = 0$: $\frac{\partial \bar{u}_1}{\partial y} = 0$, $\bar{v}_1 = 0$, $\frac{\partial \bar{\phi}_0}{\partial y} = 0$, $\frac{\partial \bar{\phi}_{10}}{\partial y} = 0$

At $y = \pm 1$: $\bar{u}_1 = 0$, $\bar{v}_1 = 0$, $\bar{\phi}_0 = 0$, $\bar{\phi}_{10} = 0$

The density, ρ_1, comes directly from the solution of the equation of state (Equation 3.35). That leaves three equations and four unknowns which, at first glance, are impossible to solve. However, a fourth equation is obtained when applying one of the boundary conditions to the continuity equation (Equation 3.32). When applying the condition that $\bar{v}_1 = 0$ at y=0, an equation for $\bar{p}_1(x)$ results. Then, using the appropriate boundary conditions for $\bar{p}_1$, the function, $\bar{p}_1(x)$, is determined explicitly. The expression for $\bar{p}_1(x)$ is then utilized in the remaining equations to solve explicitly for the remaining unknowns, $\bar{u}_1$, $\bar{\phi}_0$, $\bar{\rho}_1$, and $\bar{v}_1$.

Using standard methods of solving partial differential equations (such as separation of variables), Equations 3.32, 3.33, 3.34, and 3.35 were solved. Some simplifying substitutions were also made. Since the reference temperature is defined to

be $\Delta T_{ref} \equiv \frac{V_0^2}{2c_p}$, the Eckert number, as defined in Equation 3.9, is simply unity. Also, for an ideal gas, the quantity, $\beta_m T_m$ is approximately unity. Thus, the leading order solutions are given by the following expressions:

$$\bar{u}_1(x,y) = i\frac{d\bar{p}_1}{dx}[1 - \frac{\cosh((1+i)\eta_0 y)}{\cosh((1+i)\eta_0)}] \tag{3.36}$$

$$\bar{\phi}_0(x,y) = 2\bar{p}_1(x)[1 - \frac{\cosh((1+i)\eta_0 y\sqrt{\Pr})}{\cosh((1+i)\eta_0 y\sqrt{\Pr})}] \tag{3.37}$$

$$\bar{\rho}_1(x,y) = \bar{p}_1(x)[1 + \frac{\cosh((1+i)\eta_0 y\sqrt{\Pr})}{\cosh((1+i)\eta_0\sqrt{\Pr})}] \tag{3.38}$$

$$\begin{aligned}\bar{v}_1(x,y) = i\bar{p}_1(x)[(1-y) + (\gamma-1)(&\frac{\tanh((1+i)\eta_0\sqrt{\Pr})}{(1+i)\eta_0\sqrt{\Pr}} \\ &- \frac{\sinh((1+i)\eta_0 y\sqrt{\Pr})}{(1+i)\eta_0\sqrt{\Pr}\cosh((1+i)\eta_0\sqrt{\Pr})})] - i\frac{d^2\bar{p}_1}{dx^2}[(y-1) \\ &+ (\frac{\tanh((1+i)\eta_0)}{(1+i)\eta_0} - \frac{\sinh((1+i)\eta_0 y)}{(1+i)\eta_0\cosh((1+i)\eta_0)})]\end{aligned} \tag{3.39}$$

D. THE PRESSURE DISTRIBUTION

Applying the boundary condition that $\bar{v}_1 = 0$ at y=0 to the continuity equation (Equation 3.32), an ordinary second order differential equation for $\bar{p}_1(x)$ results as follows:

$$\frac{d^2\bar{p}_1}{dx^2} + m^2\bar{p}_1(x) = 0 \qquad \text{where}$$

$$m^2 = \frac{[1 + (\gamma-1)(\frac{\tanh((1+i)\eta_0\sqrt{\Pr})}{(1+i)\eta_0\sqrt{\Pr}})]}{[1 - (\frac{\tanh((1+i)\eta_0)}{(1+i)\eta_0})]} \tag{3.40}$$

The boundary conditions necessary for determining $\bar{p}_1(x)$ are found in the geometry of the problem. As shown in Figure 3.1, the plates are flush with the source of the acoustic wave at x=0. This means that the pressure amplitude is at a peak (magnitude of one), and the velocity amplitude, and therefore the pressure gradient, is at a node (magnitude of zero). Thus, the appropriate boundary conditions needed for determining the pressure distribution are at x=0, $\bar{p}_1 = i$ and $\frac{d\bar{p}_1}{dx} = 0$. Solving for $\bar{p}_1(x)$ and applying these boundary conditions, the result is

$$\bar{p}_1(x) = i\cos(mx) \tag{3.41}$$

This expression is then substituted back into Equations 3.36, 3.37, 3.38, and 3.39 to give explicit forms of $\bar{u}_1, \bar{\phi}_0, \bar{p}_1$, and $\bar{v}_1$ respectively.

The two cases studied in this research are the wide gap and arbitrary gap cases which differ bases on the width of separation between the plates as compared to the Stokes's boundary layer thickness as discussed in Chapter I. The basic assumption that is made in the wide gap case is that, in the pressure distribution of Equation 3.41, the parameter "m" is assumed to be unity since $m \approx 1$. This simplifies the problem significantly, since the pressure distribution just varies as cos(x) and is independent of any other parameter. For the arbitrary gap case, "m", is left as a function of η_0, γ, and Pr as shown in Equation 3.40, and the pressure distribution becomes dependent upon those three parameters as well as on the variable, x.

E. HIGHER ORDER BEHAVIOR

The higher order velocity, density, and pressure terms, $\bar{u}_2, \bar{\rho}_2, \bar{v}_2$ and $\bar{p}_2$, and higher will not be considered in this study; however, the higher order temperature term, $\bar{\phi}_1$, is significant and will be considered in this section. The equation to be solved in this consideration is the O(1) energy equation:

Energy: O(1):

$$\frac{\partial \phi_1}{\partial t} + \rho_1 \frac{\partial \phi_0}{\partial t} + u_1 \frac{\partial \phi_0}{\partial x} + v_1 \frac{\partial \phi_0}{\partial y} = \frac{1}{2\eta_0^2 \,\mathrm{Pr}} \frac{\partial^2 \phi_1}{\partial y^2} + 2\beta T_m Ec \frac{\Delta T_{ref}}{T_m} (\phi_0 \frac{\partial p_3}{\partial t} + \phi_1 \frac{\partial p_2}{\partial t} + \phi_2 \frac{\partial p_1}{\partial t} + \phi_0 u_1 \frac{\partial p_2}{\partial x} + \phi_0 u_2 \frac{\partial p_1}{\partial x} + \phi_1 u_1 \frac{\partial p_1}{\partial x}) + 2\beta T_m Ec \frac{\partial p_2}{\partial t} + 2\beta T_m Ec u_1 \frac{\partial p_1}{\partial x} + \frac{Ec}{\eta_0^2} (\frac{\partial u_1}{\partial y})^2 \tag{3.42}$$

Again applying the equality, $\frac{\Delta T_{ref}}{T_m} = M^2(\frac{\gamma - 1}{2})$, and subsequently neglecting terms of order M^2, Equation 3.42 further reduces to

Energy: O(1):

$$\frac{\partial \phi_1}{\partial t} + \rho_1 \frac{\partial \phi_0}{\partial t} + u_1 \frac{\partial \phi_0}{\partial x} + v_1 \frac{\partial \phi_0}{\partial y} = \frac{1}{2\eta_0^2 \,\mathrm{Pr}} \frac{\partial^2 \phi_1}{\partial y^2} + 2\beta T_m Ec \frac{\partial p_2}{\partial t} + 2\beta T_m Ec u_1 \frac{\partial p_1}{\partial x} + \frac{Ec}{\eta_0^2} (\frac{\partial u_1}{\partial y})^2 \tag{3.43}$$

Equation 3.43 is not complete; it is missing one term. The extra term comes from expanding the coefficient of thermal expansion, β, into its perturbation form. By definition,

$$\beta = -\frac{1}{\rho^*} (\frac{\partial \rho^*}{\partial T^*})_p = -\frac{1}{\rho^*} [(\frac{\partial \rho^*}{\partial T^*})_m + (\frac{\partial^2 \rho^*}{\partial T^{*2}})_m \Delta T^* + \ldots \tag{3.44}$$

where: $\Delta T^* = T^* - T_m = \phi \Delta T_{ref}$

Utilizing the appropriate scaling factors for ρ^* and T^* from Equation 3.5, and the corresponding perturbation solution forms from Equation 3.11, the expanded equation for βT^* becomes

$$\beta T^* = \beta_m T_m \{1 - M[\rho_1 + \phi_0 \frac{c^2}{2c_p T_m}(\frac{T_m}{\rho_m \beta_m}(\frac{\partial^2 \rho^*}{\partial T^{*2}}) - 1] + 0(M^2) + \ldots\} \qquad (3.45)$$

Since $\frac{T_m}{\rho_m \beta_m}(\frac{\partial^2 \rho^*}{\partial T^{*2}}) = 2$ for an ideal gas, and $\frac{c^2}{2c_p T_m} = \frac{\gamma - 1}{2}$, Equation 3.45 simplifies to

$$\beta T^* = \beta_m T_m \{1 - M[\rho_1 + (\frac{\gamma - 1}{2})\phi_0 + 0(M^2) + \ldots\} \qquad (3.46)$$

Substituting the expanded βT^* expression into the energy perturbation equation, an extra O(1) term comes out of the $2Ec\beta T^*(\frac{1}{M})\frac{\partial p}{\partial t}$ term from the O(M) portion of βT multiplying with ($1/M$). Therefore, the extra O(1) energy term is $-2\beta_m T_m[\rho_1 \frac{\partial p_1}{\partial t} + (\frac{\gamma - 1}{2})\phi_0 \frac{\partial p_1}{\partial t}]$, making the complete O(1) energy equation as follows:

Energy: O(1):

$$\frac{\partial \phi_1}{\partial t} + \rho_1 \frac{\partial \phi_0}{\partial t} + u_1 \frac{\partial \phi_0}{\partial x} + v_1 \frac{\partial \phi_0}{\partial y} = \frac{1}{2\eta_0^2 \,\mathrm{Pr}} \frac{\partial^2 \phi_1}{\partial y^2} + 2\beta_m T_m Ec \frac{\partial p_2}{\partial t} \qquad (3.47)$$
$$+ 2\beta_m T_m Ec u_1 \frac{\partial p_1}{\partial x} + \frac{Ec}{\eta_0^2}(\frac{\partial u_1}{\partial y})^2 - 2\beta_m T_m[\rho_1 \frac{\partial p_1}{\partial t} + (\frac{\gamma - 1}{2})\phi_0 \frac{\partial p_1}{\partial t}]$$

Substituting the relations from Equation 3.17 into Equation 3.47, yields the following complex partial differential equation:

Energy: $O(1)$:

$$\begin{aligned}\mathrm{Re}[2i\bar{\phi}_{12}e^{2it} + i\bar{\rho}_1\bar{\phi}_0 e^{2it} + \bar{u}_1\frac{\partial\bar{\phi}_0}{\partial x}e^{2it} + \bar{v}_1\frac{\partial\bar{\phi}_0}{\partial y}e^{2it}] &= \frac{1}{2\eta_0^2\,\mathrm{Pr}}\frac{\partial^2\phi_{10}}{\partial y^2} \\ + \mathrm{Re}[\frac{1}{2\eta_0^2\,\mathrm{Pr}}\frac{\partial^2\bar{\phi}_{12}}{\partial y^2}e^{2it} + 4Ec\beta_m T_m i\bar{p}_2 e^{2it} + \frac{Ec}{\eta_0^2}(\frac{\partial\bar{u}_1}{\partial y})^2 e^{2it} & \\ + 2Ec\beta_m T_m\bar{u}_1\frac{d\bar{p}_1}{dx}e^{2it} - 2\beta_m T_m i\bar{\rho}_1\bar{p}_1 e^{2it} - \beta_m T_m i(\gamma-1)\bar{\phi}_0\bar{p}_1 e^{2it}] &\end{aligned} \tag{3.48}$$

Two equations may be extracted from Equation 3.48. One yields information about the first harmonic of $\bar{\phi}_1$, which is the real variable, ϕ_{10}; solution of the other equation yields the second harmonic, $\bar{\phi}_{12}$, which is complex. The determination of $\bar{\phi}_{12}$ is not of interest in this study since it does not contain a steady temperature component; however, ϕ_{10} is the time-averaged temperature. Since it is of great importance to this research, the time-averaged temperature, ϕ_{10}, is considered in detail in the next section.

F. THE TIME-AVERAGED TEMPERATURE, ϕ_{10}

In Equation 3.48, there is one term which obviously has no time dependence, $(\frac{1}{2\eta_0^2\,\mathrm{Pr}}\frac{\partial^2\phi_{10}}{\partial y^2})$; the remaining terms are multiplied by e^{2it}. This supposed time dependence would imply a simple solution for ϕ_{10} since it would mean that $\frac{\partial^2\phi_{10}}{\partial y^2} = 0$. However, upon close inspection of the e^{2it} terms, it is noted that most of them have a steady (time independent) term embedded in them. Taking the time average of Equation 3.48, the only terms which drop out (average to zero) are $2i\bar{\phi}_{12}e^{2it}$,

$\frac{1}{2\eta_0^2 \mathrm{Pr}} \frac{\partial^2 \bar{\phi}_{12}}{\partial y^2} e^{2it}$, and $4Ec\beta_m T_m i\bar{p}_2 e^{2it}$, leaving the equation to be solved for the first harmonic as (angle brackets < > denote time average):

Energy - $O(1)$ 1st harmonic:

$$< i\bar{\rho}_1 \bar{\phi}_0 > + < \bar{u}_1 \frac{\partial \bar{\phi}_0}{\partial x} > + < \bar{v}_1 \frac{\partial \bar{\phi}_0}{\partial y} >= \frac{1}{2\eta_0^2 \mathrm{Pr}} \frac{\partial^2 \phi_{10}}{\partial y^2} + < \frac{Ec}{\eta_0^2} (\frac{\partial \bar{u}_1}{\partial y})^2 > \qquad (3.49)$$

$$+ < 2Ec\beta_m T_m \bar{u}_1 \frac{d\bar{p}_1}{dx} > - < 2\beta_m T_m i\bar{\rho}_1 \bar{p}_1 > - < \beta_m T_m i(\gamma - 1)\bar{\phi}_0 \bar{p}_1 >$$

The equation for ϕ_{10} (Equation 3.49) involves time averages. The time average of a product of two complex variables is given by the following expression:

$$< \bar{f}\,\bar{g} >= \frac{1}{2} \mathrm{Re}[\bar{f}\,\bar{g}^{**}] \qquad (3.50)$$

where $\bar{g}^{**}$ is the complex conjugate of $\bar{g}$. Applying this definition to all of the time average terms in Equation 3.49 results in an equation for $\frac{\partial^2 \phi_{10}}{\partial y^2}$ which then must be integrated twice to find an expression for ϕ_{10}. The procedure is fairly straightforward; however, the calculus and algebraic manipulations involved in solving the equation by hand are extremely cumbersome. For example, evaluating the time average of the first term, $< i\bar{\rho}_1 \bar{\phi}_0 >$, is accomplished using the definition of time average from Equation 3.50 and substituting into it the expressions for $\bar{\rho}_1$ and $\bar{\phi}_0$ from Equations 3.37, 3.38, and 3.41 as follows:

$$< \bar{\rho}_1 i\bar{\phi}_0 >= \frac{1}{2}\mathrm{Re}[\bar{\rho}_1(-i)\bar{\phi}_0 **] = \frac{1}{2}\mathrm{Re}\{i\cos(mx)[1+\frac{\cosh((1+i)\eta_0 y\sqrt{\mathrm{Pr}})}{\cosh((1+i)\eta_0\sqrt{\mathrm{Pr}})}]*$$

$$(-i)[2i\cos(mx)(1-\frac{\cosh((1+i)\eta_0 y\sqrt{\mathrm{Pr}})}{\cosh((1+i)\eta_0\sqrt{\mathrm{Pr}})})]**\} \qquad (3.51)$$

$$\text{where } m = \sqrt{\frac{[1+(\gamma-1)(\frac{\tanh((1+i)\eta_0\sqrt{\mathrm{Pr}})}{(1+i)\eta_0\sqrt{\mathrm{Pr}}})]}{[1-(\frac{\tanh((1+i)\eta_0)}{(1+i)\eta_0})]}}$$

Once the complex conjugate of $\bar{\phi}_0$ is correctly computed, the real part of the entire expression must be evaluated without error. This establishes the first time average term, but there are six more which must be obtained in a similar fashion. The summation of all seven resulting time average terms must then be integrated twice, applying appropriate boundary conditions, to obtain an expression for ϕ_{10}. The vast amount of careful mathematical manipulation and computation required to solve for ϕ_{10} points directly to the use of a powerful symbolic mathematical software tool. Thus, MAPLE, just such a computer software package, is utilized to solve for ϕ_{10}, given all of the other expressions for $\bar{u}_1$, $\bar{\phi}_0$, $\bar{\rho}_1$, $\bar{v}_1$, and $\bar{p}_1$. ϕ_{10} is found first for the simpler wide gap case and then for the arbitrary gap case. The resulting expressions for ϕ_{10} are much too lengthy to include explicitly in this paper; however, the temperature distributions described by ϕ_{10} are plotted and discussed in Chapter IV.

IV. RESULTS AND DISCUSSION

The results of this work are comprised of the solutions to the governing equations as given in Chapter III along with plots of these solutions. These plots are presented and discussed in the following sections for different values of $\eta_0\sqrt{\mathrm{Pr}} = \frac{y_0}{\delta_\alpha}$ where the thermal penetration depth is $\delta_\alpha = \sqrt{\frac{2\alpha}{\omega}} = \frac{\delta_v}{\sqrt{\mathrm{Pr}}}$. The parameter, $\eta_0\sqrt{\mathrm{Pr}}$, has been found to be the more appropriate gap width parameter than η_0 in dealing with thermal effects in such oscillatory flow problems. Since the form of the leading order pressure distribution, $\overline{p}_1(x)$, is crucial in determining the behavior of the remaining leading order solutions and the higher order solutions, the pressure distribution results are analyzed first. Then, the leading order velocity, temperature, and density solutions and the higher order time-averaged temperature term are presented. Finally, the recovery factor, suitably defined for this model problem, is presented, plotted and discussed.

A. THE PRESSURE DISTRIBUTION

The pressure distribution, $\overline{p}_1(x)$, for this model problem is found, as given in Chapter III, as

$$p_1(x,t) = \mathrm{Re}[\overline{p}_1(x)e^{it}], \text{ where } \overline{p}_1(x) = i\cos(mx) \text{ and}$$

$$m = \sqrt{\frac{[1+(\gamma-1)(\frac{\tanh((1+i)\eta_0\sqrt{\mathrm{Pr}})}{(1+i)\eta_0\sqrt{\mathrm{Pr}}})]}{[1-(\frac{\tanh((1+i)\eta_0)}{(1+i)\eta_0})]}} \qquad (4.1)$$

Note that the eigenvalue "*m*" is in general complex; however, with increasing gap width, the parameter "*m*" approaches a value of one. Therefore, in the idealized wide gap case, it is assumed that *m*=1, and the pressure distribution is a simple cosine function, i.e. $\overline{p}_1(x) = i\cos x$ and $p_1(x,t) = -\cos x \sin t$. In general, for the arbitrary gap case, "*m*" is a complex number, $m = a - bi$. As gap width (or η_0) increases, "*a*" reduces to a value of one and "*b*" to a value of zero, approaching the results of the idealized wide gap case. For all of the trials calculated, the values of "*m*" are given in Table 4.1. The value of "*m*" also depends on the gas properties, γ and Pr. Thus, for the same η_0 value or gap width, the magnitude of "*m*" will vary for different gases. The ideal gas utilized in this work is air; therefore, the property values used are γ=1.4 and Pr=0.7.

Table 4.1 Values of "*m*" in Pressure Distribution.

$\eta_0\sqrt{\text{Pr}}$	*m*	|*m*|
1	1.3047-0.5939*i*	1.443
1.5	1.1814-0.3165*i*	1.223
2	1.1405-0.2055*i*	1.159
3	1.1002-0.1229*i*	1.107
4	1.0762-0.0884*i*	1.080
5	1.0613-0.0688*i*	1.064

Two plots of the pressure distribution, $p_1(x,t)$, are given in Figure 4.1, for $\eta_0\sqrt{\text{Pr}}$ values of 1.5 and 5. Considering the $\eta_0\sqrt{\text{Pr}}$ =5 case, the pressure distribution closely resembles the idealized wide gap case of $p_1(x,t) = -\cos x \sin t$. As gap width decreases, the amplitude of the cosine function increases, and the waveform is considerably distorted

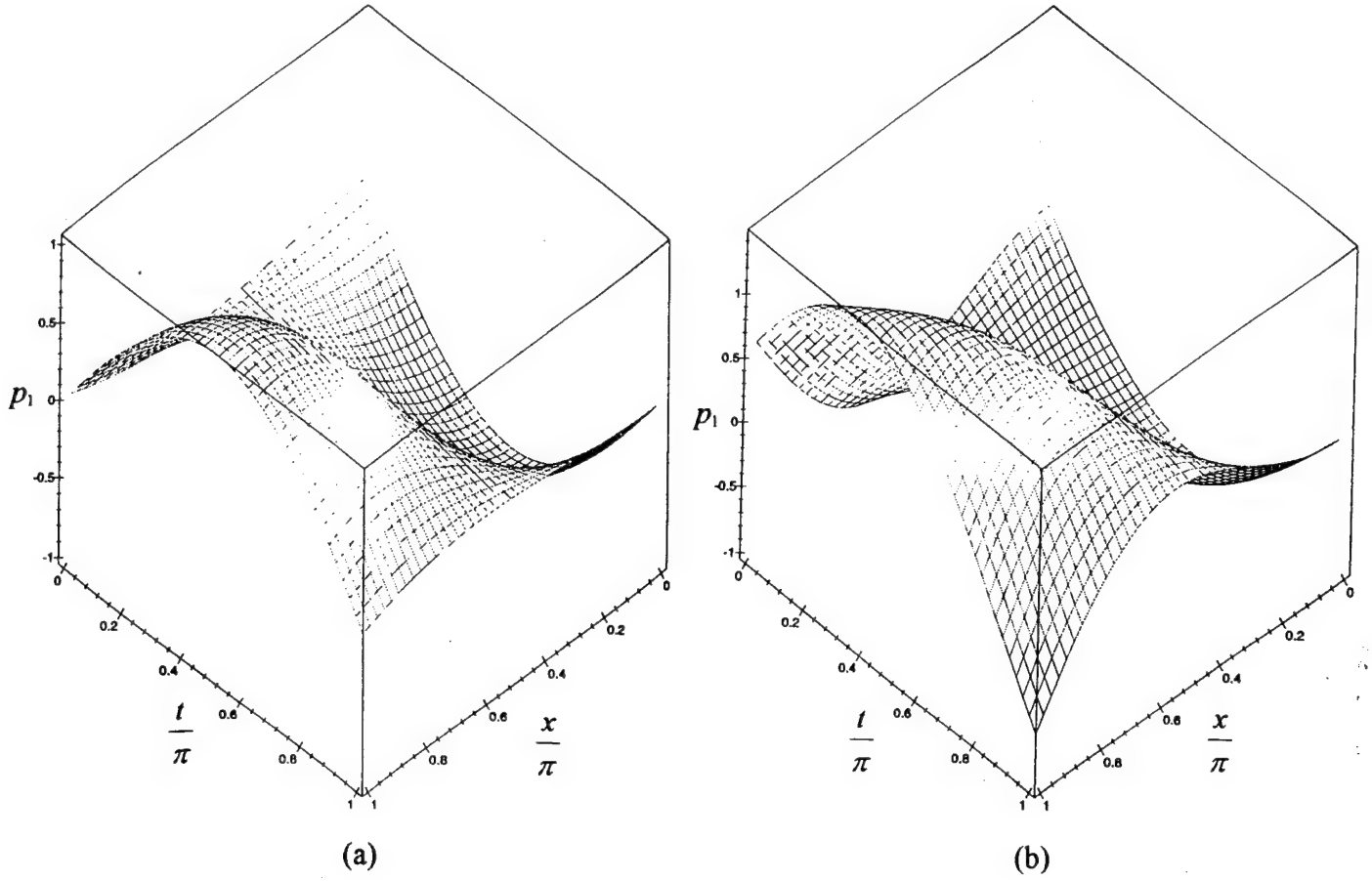

Figure 4.1 Pressure Distribution, $p_1(x,t)$, for (a) $\eta_0\sqrt{\text{Pr}} = 5$ and (b) $\eta_0\sqrt{\text{Pr}} = 1.5$

as illustrated by the $\eta_0\sqrt{\mathrm{Pr}}=1.5$ plot. This variation in amplitude is clearly observed in Figure 4.2 where $p_1(x,t)$ is plotted at two particular times $t=\frac{\pi}{2}$ and $t=\pi$ for $\eta_0\sqrt{\mathrm{Pr}}$ values of 1.5, 2, 3 and 5. To emphasize the distortion as compared to the idealized wide gap case, the function, $p_1(x,t)=-\cos x \sin t$ is also plotted in Figure 4.2. Based on the calculated values of "m" and the plots of the pressure distributions, the gap width corresponding to $\eta_0\sqrt{\mathrm{Pr}}=5$ is determined to the sufficiently close to the idealized wide gap case to be considered as a "wide gap". Again as η_0 decreases into the "narrow gap" region ($\eta_0\sqrt{\mathrm{Pr}}<5$), the pressure distribution significantly deviates from the simple cos(x) behavior of the idealized wide gap case.

B. LEADING ORDER BEHAVIOR

The leading order first harmonic solutions for the primary variables (velocity components, temperature and density) are given as follows (as discussed in Chapter III): $u_1(x,y,t)=\mathrm{Re}[\bar{u}_1(x,y)e^{it}]$, $\phi_0(x,y,t)=\mathrm{Re}[\bar{\phi}_0(x,y)e^{it}]$, $\rho_1(x,y,t)=\mathrm{Re}[\bar{\rho}_1(x,y)e^{it}]$, and $v_1(x,y,t)=\mathrm{Re}[\bar{v}_1(x,y)e^{it}]$, where

$$\bar{u}_1(x,y)=i\frac{d\bar{p}_1}{dx}\left[1-\frac{\cosh((1+i)\eta_0 y)}{\cosh((1+i)\eta_0)}\right] \tag{4.2}$$

$$\bar{\phi}_0(x,y)=2\bar{p}_1(x)\left[1-\frac{\cosh((1+i)\eta_0 y\sqrt{\mathrm{Pr}})}{\cosh((1+i)\eta_0\sqrt{\mathrm{Pr}})}\right] \tag{4.3}$$

$$\bar{\rho}_1(x,y)=\bar{p}_1(x)\left[\gamma-(\gamma-1)\left(1-\frac{\cosh((1+i)\eta_0 y\sqrt{\mathrm{Pr}})}{\cosh((1+i)\eta_0\sqrt{\mathrm{Pr}})}\right)\right] \tag{4.4}$$

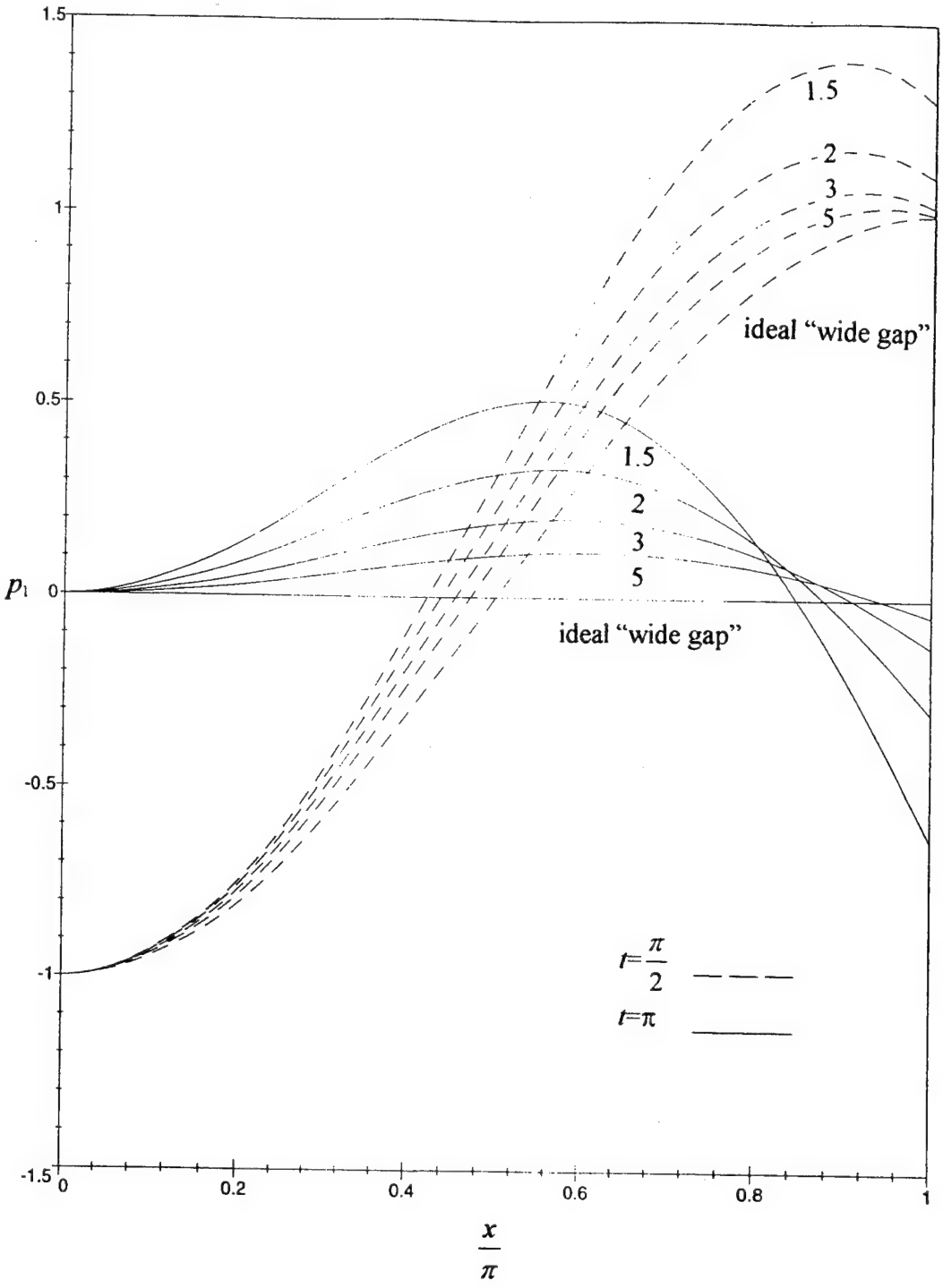

Figure 4.2 Pressure, $p_1(x,t)$, for $t=\frac{\pi}{2}$ and $t=\pi$, for $\eta_0\sqrt{\mathrm{Pr}}$ = 1.5, 2, 3, and 5

$$\bar{v}_1(x,y) = i\bar{p}_1(x)[(1-y)+(\gamma-1)(\frac{\tanh((1+i)\eta_0\sqrt{\Pr})}{(1+i)\eta_0\sqrt{\Pr}} - \frac{\sinh((1+i)\eta_0 y\sqrt{\Pr})}{(1+i)\eta_0\sqrt{\Pr}\cosh((1+i)\eta_0\sqrt{\Pr})})] - i\frac{d^2\bar{p}_1}{dx^2}[(y-1) + (\frac{\tanh((1+i)\eta_0)}{(1+i)\eta_0} - \frac{\sinh((1+i)\eta_0 y)}{(1+i)\eta_0\cosh((1+i)\eta_0)})] \quad (4.5)$$

These quantities, as opposed to the pressure distribution, depend on both spatial variables, x and y. Their x dependence is given by either $\cos(mx)$ or $\sin(mx)$ which stems from their dependence on the pressure distribution or the pressure gradient. Because of this periodicity in x, all of the information about the x dependence of a particular leading order distribution is contained in an interval of one half of the wavelength (i.e. $0 \le x \le \pi$). In the y direction, the quantities u_1, ϕ_0, and ρ_1 are symmetric about the centerline of the channel (y=0), whereas the velocity in the y direction, v_1, is antisymmetric about the centerline. Therefore, the results for all of these distributions are determined and presented for one half of the channel only, specifically for $0 \le y \le 1$. The plots of the leading order density distribution, $\rho_1(x,y,t)$, are not included in the discussion since the behavior of the density function is not of direct interest to this work.

The velocity distribution, $u_1(x,y,t)$, is given in Figure 4.3 for $x=\pi$ and $\eta_0\sqrt{\Pr}$ values of 1.5 and 5. $u_1(x,y,t)$ depends on the pressure gradient; therefore, it varies in x as $\sin(mx)$. This distribution, as observed in Equation 4.2, varies in y as $\mathrm{Re}[1-\frac{\cosh((1+i)\eta_0 y)}{\cosh((1+i)\eta_0)}]$. Figure 4.4 shows $u_1(x,y,t)$ for $x=\pi$ at two instants in time, $t=\frac{\pi}{2}$ and $t=\pi$ for $\eta_0\sqrt{\Pr}$ = 1.5, 2, 3, and 5. The distributions clearly show that the velocity vanishes at the wall (y=1) and thereby satisfies the no slip condition. Also, because

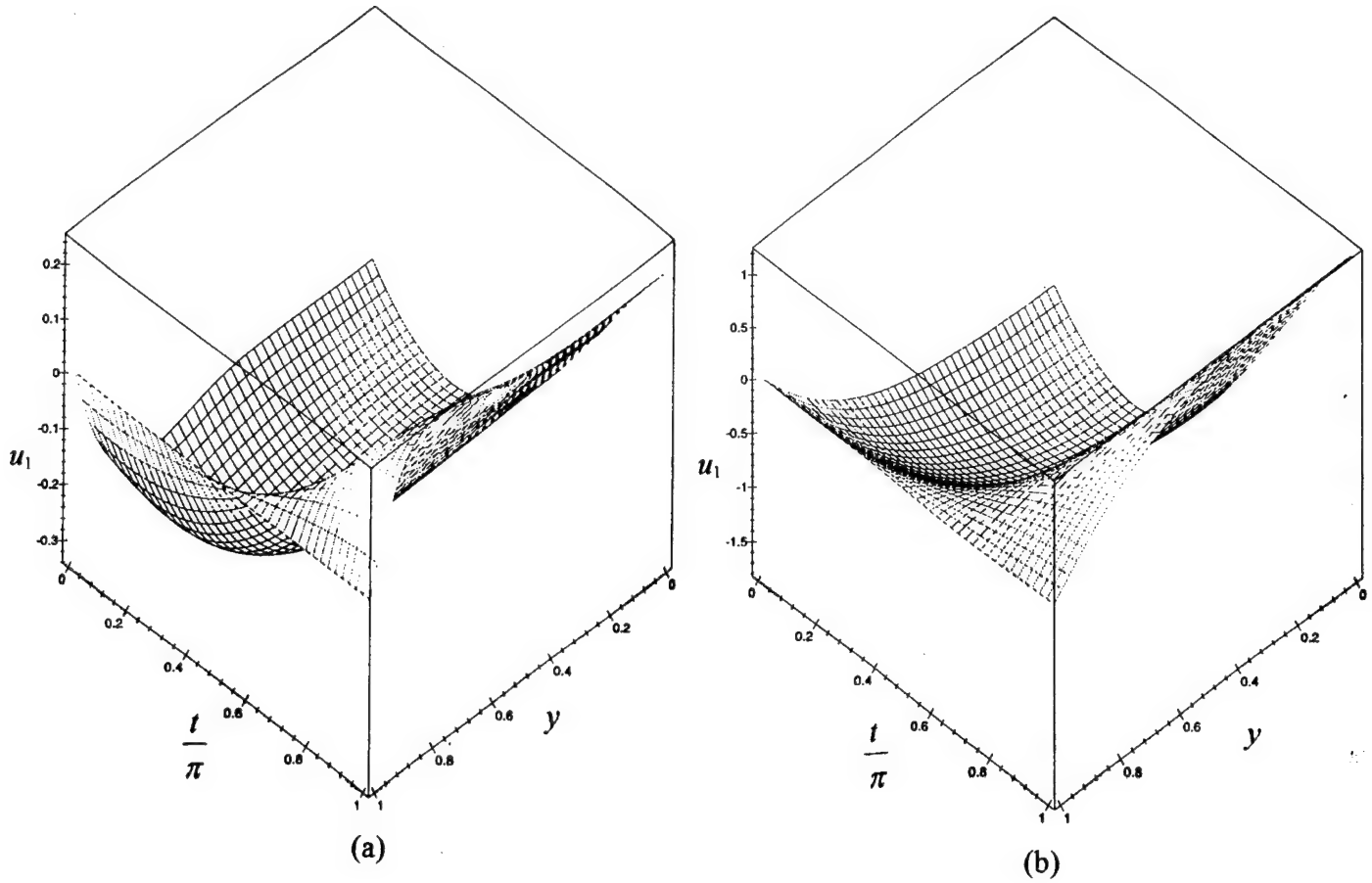

Figure 4.3 Velocity Distribution, $u_1(x,y,t)$, for $x=\pi$ and for (a) $\eta_0\sqrt{\mathrm{Pr}} = 5$ and (b) $\eta_0\sqrt{\mathrm{Pr}} = 1.5$

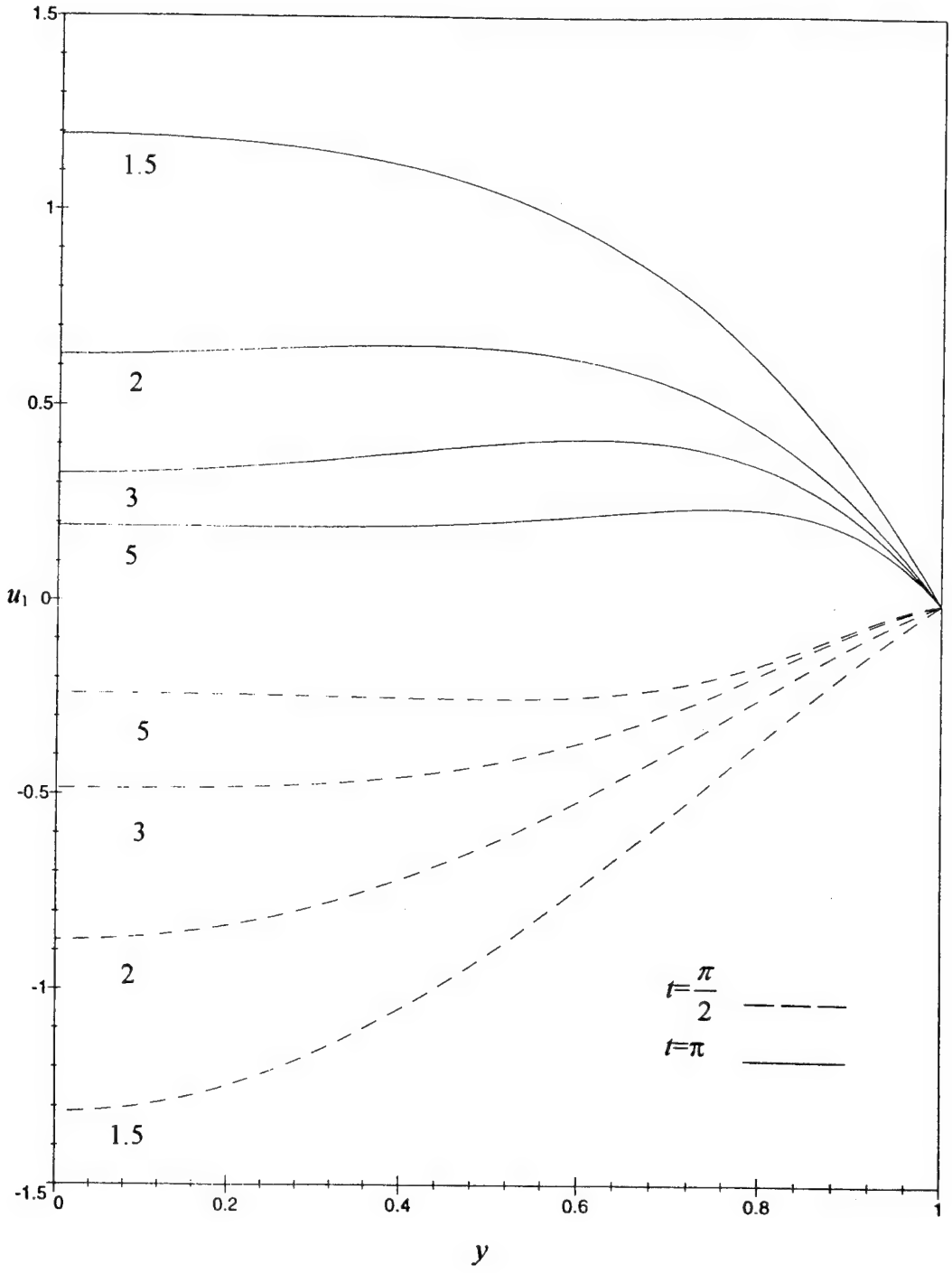

Figure 4.4 Velocity Distribution, $u_1(x,y,t)$, for $x=\pi$, for $t=\frac{\pi}{2}$ and $t=\pi$, and for $\eta_0\sqrt{\mathrm{Pr}}$ = 1.5, 2, 3, and 5

$u_1(x,y,t)$ is symmetric about the centerline of the channel, the gradient there is equal to zero as shown by the zero slope at y=0. For wide gaps or large values of η_0, the velocity component, u_1, increases in magnitude from zero at the wall (y=1) to a maximum value and then decreases slightly to level off with a slope of zero at the centerline (y=0). As the gap narrows or η_0 decreases, the u_1 velocity value increases, and the location of the peak velocity in the channel shifts toward the centerline. In fact, for $\eta_0\sqrt{\mathrm{Pr}}$ =1.5, the maximum velocity value occurs at the centerline, and the distribution is more parabolic in shape (similar to that of Poiseuille flow). These trends are clearly observed in the curves for both snapshots in time, $t=\frac{\pi}{2}$ and $t=\pi$, in Figure 4.4.

The leading order temperature solution, $\phi_0(x,y,t)$, is illustrated in Figure 4.5 for $x=\pi$ and $\eta_0\sqrt{\mathrm{Pr}}$ = 1.5 and 5. The x dependence is a cosine function, $i\cos(mx)$, which is caused by the direct relationship of ϕ_0 to the pressure distribution. The y dependence of ϕ_0 is of the form $\mathrm{Re}[i(1-\frac{\cosh((1+i)\eta_0 y\sqrt{\mathrm{Pr}})}{\cosh((1+i)\eta_0\sqrt{\mathrm{Pr}})})]$ as observed in Equation 4.3. In Figure 4.6, where ϕ_0 is plotted for $x=\pi$, at two instants in time, $t=\frac{\pi}{2}$ and $t=\pi$, and for $\eta_0\sqrt{\mathrm{Pr}}$ values of 1.5, 2, 3, and 5, the dependence of ϕ_0 on y and η_0 is displayed, and its similarity to that of the u_1 velocity distribution is noted. The boundary conditions of no slip at the wall and symmetry at the centerline are clearly met as ϕ_0=0 at y=1 and its slope vanishes at y=0. Considering the curves for time $t=\pi$, for large gap widths or η_0 values, the temperature, ϕ_0, increases in magnitude from zero at the wall to a peak and then decreases to the centerline temperature value which is approached at zero slope. Again, as the gap

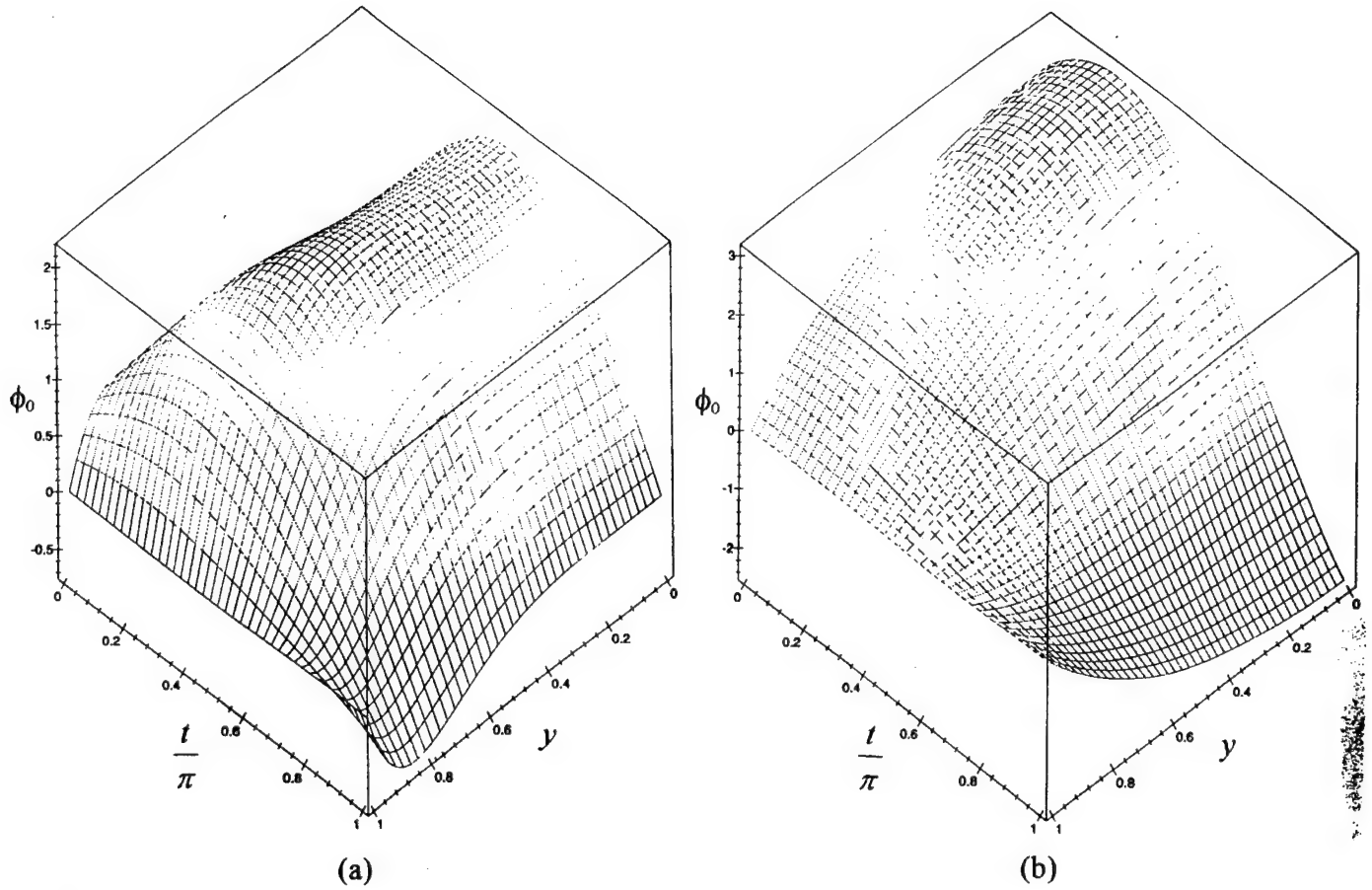

Figure 4.5 Temperature Distribution, $\phi_0(x,y,t)$, for $x=\pi$ and for (a) $\eta_0\sqrt{\mathrm{Pr}} = 5$ and (b) $\eta_0\sqrt{\mathrm{Pr}} = 1.5$

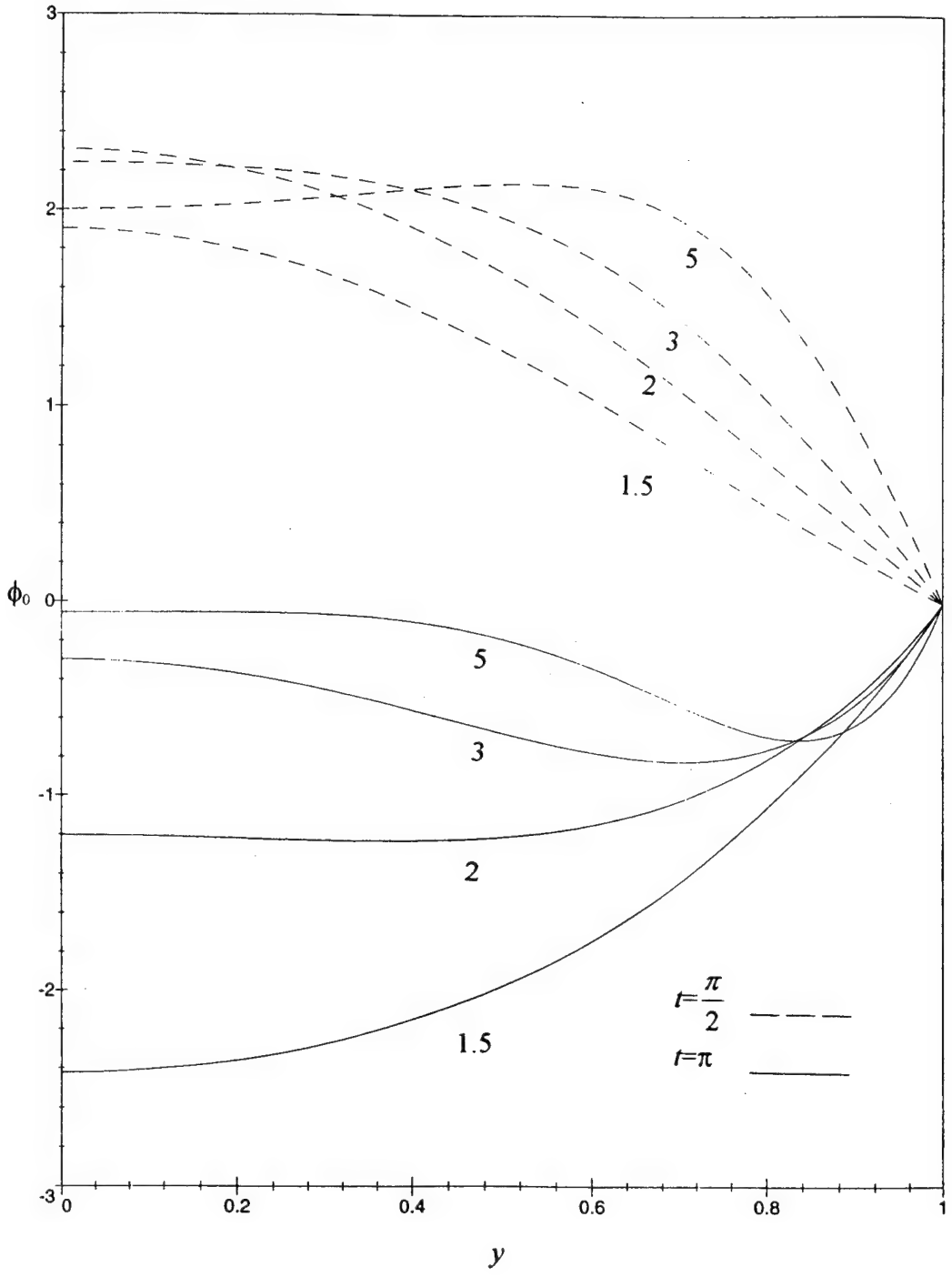

Figure 4.6 Temperature Distribution, $\phi_0(x,y,t)$, for $x=\pi$, for $t=\frac{\pi}{2}$ and $t=\pi$, and for $\eta_0\sqrt{\mathrm{Pr}}$ = 1.5, 2, 3, and 5

width or η_0 value decreases, the peak shifts toward the centerline and its magnitude increases. As with the u_1 velocity component, the shape of this temperature distribution becomes more parabolic as the gap narrows or η_0 decreases. The dependence of the temperature, ϕ_0, on gap width or η_0 is not accurately portrayed in the plots for time, $t=\frac{\pi}{2}$. This is explained by the nature of the time dependence of the temperature distribution, $\phi_0(x,y,t)$. A phase lag occurs in time, and the amount of this phase lag depends on the value of η_0; therefore, the temperature distributions at the instant of time, $t=\frac{\pi}{2}$, for the different gap widths do not correspond to the same time positions in their respective periods.

The velocity component in the y direction, $v_1(x,y,t)$, is presented in Figure 4.7 for $x=\pi$ and $\eta_0\sqrt{Pr}$ = 1.5 and 5. From Equation 4.5, it is observed that $v_1(x,y,t)$ depends on both the pressure distribution and its second derivative. Therefore, the x dependence is a cosine function, $\cos(mx)$. The y dependence of $v_1(x,y,t)$ is a combination of linear terms, hyperbolic sine terms and constants, resulting in a function which is antisymmetric about $y=0$. In Figure 4.8, $v_1(x,y,t)$ is plotted for $x=\pi$, at two instants in time, $t=\frac{\pi}{2}$ and $t=\pi$, and for $\eta_0\sqrt{Pr}$ values of 1.5, 2, 3, and 5. The boundary conditions of no penetration at the wall and "zero crossover" at the centerline for an antisymmetric distribution are satisfied as $v_1=0$ at $y=1$ and $y=0$ respectively. The behavior change in v_1 as gap width or η_0 changes is clearly illustrated by the $t=\pi$ curves. For large gap widths, the y component of the velocity, v_1, increases in magnitude from zero at the centerline to a peak near the wall

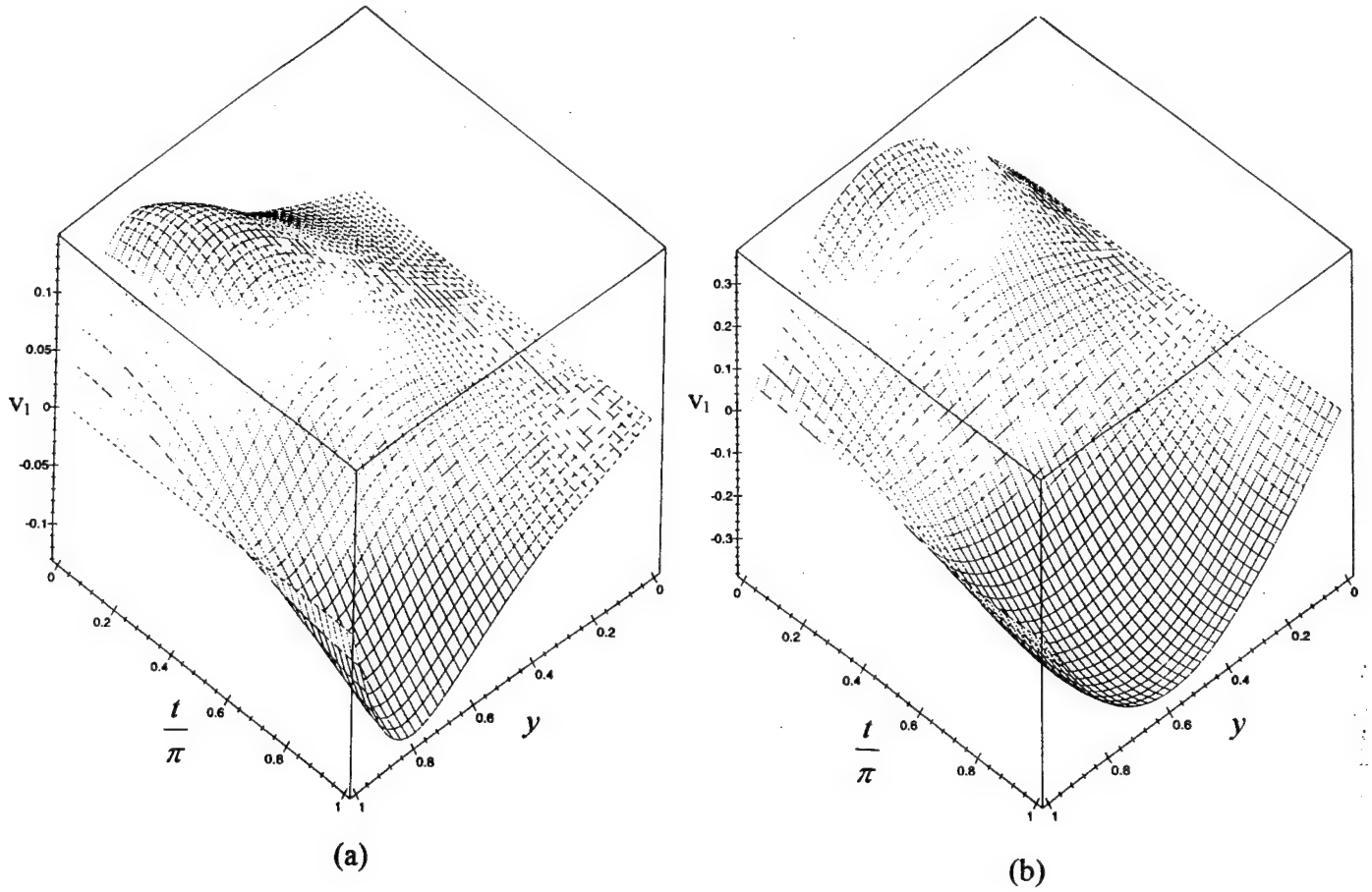

Figure 4.7 Velocity Distribution, $v_1(x,y,t)$, for $x=\pi$ and for (a) $\eta_0\sqrt{\mathrm{Pr}} = 5$ and (b) $\eta_0\sqrt{\mathrm{Pr}} = 1.5$

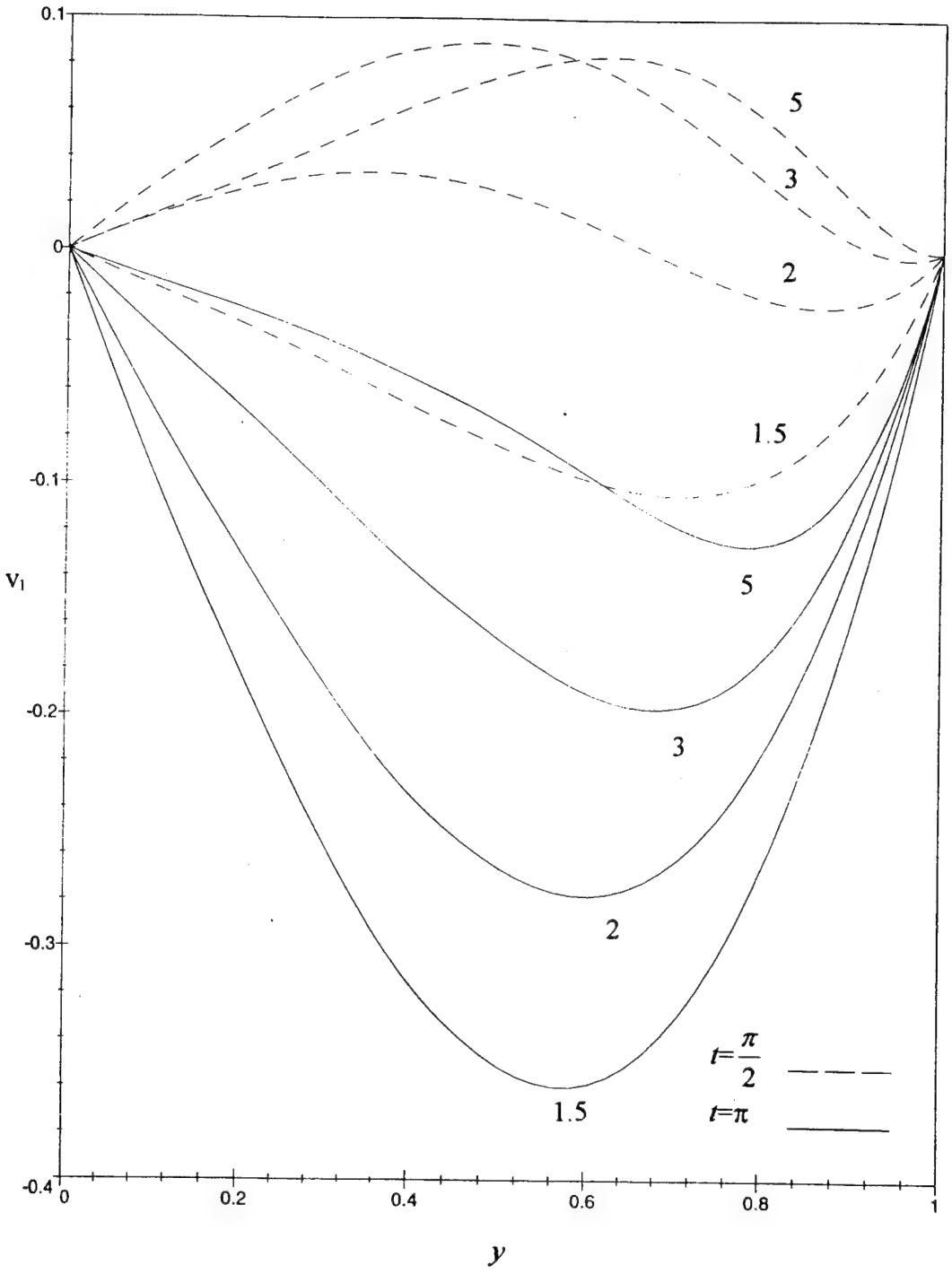

Figure 4.8 Velocity Distribution, $v_1(x,y,t)$, for $x=\pi$, for $t=\frac{\pi}{2}$ and $t=\pi$, and for $\eta_0\sqrt{\mathrm{Pr}}$ = 1.5, 2, 3, and 5

and then decreases rapidly in magnitude back to zero at the wall. An inflection point is observed between the centerline and the peak value for wide gaps. As the gap narrows or η_0 decreases, the peak increases in magnitude and shifts away from the wall. Also, the shape of the distribution becomes more parabolic for narrower gaps (i.e. the inflection point observed in the wide gap trials disappears as η_0 decreases). The trend cannot be distinguished in the $t=\frac{\pi}{2}$ plots for reasons relating to the nature of the time dependence of $v_1(x,y,t)$ which are similar to those discussed in the $\phi_0(x,y,t)$ results.

C. THE TIME-AVERAGED TEMPERATURE

The time-averaged temperature distribution, $\phi_{10}(x,y)$, is shown in Figure 4.9 for $\eta_0\sqrt{\mathrm{Pr}} = 1.5$ and 5. From the partial differential equation for ϕ_{10} as presented in Chapter III and again here for convenience,

$$\begin{aligned} &< i\bar{\rho}_1\bar{\phi}_0 > + < \bar{u}_1 \frac{\partial\bar{\phi}_0}{\partial x} > + < \bar{v}_1 \frac{\partial\bar{\phi}_0}{\partial y} > = \frac{1}{2\eta_0^2\,\mathrm{Pr}} \frac{\partial^2\phi_{10}}{\partial y^2} + < \frac{Ec}{\eta_0^2} (\frac{\partial\bar{u}_1}{\partial y})^2 > \\ &+ < 2Ec\beta_m T_m \bar{u}_1 \frac{d\bar{p}_1}{dx} > - < 2\beta_m T_m i\bar{\rho}_1\bar{p}_1 > - < \beta_m T_m i(\gamma-1)\bar{\phi}_0\bar{p}_1 > \end{aligned} \tag{4.6}$$

the x dependence is determined by the various time-averaged terms in the forcing function. The terms involve the multiplication of two of the leading order first harmonic solutions of the primary variables, u_1, ϕ_0, ρ_1 , and v_1, or their derivatives. Substituting the appropriate distributions from Equations 4.2, 4.3, 4.4, and 4.5 into Equation 4.6, the x dependence of ϕ_{10} is observed to stem from terms where the pressure distribution is multiplied by itself as well as terms where the pressure gradient is multiplied by itself. Therefore, the resulting time-averaged temperature distribution varies in x as a

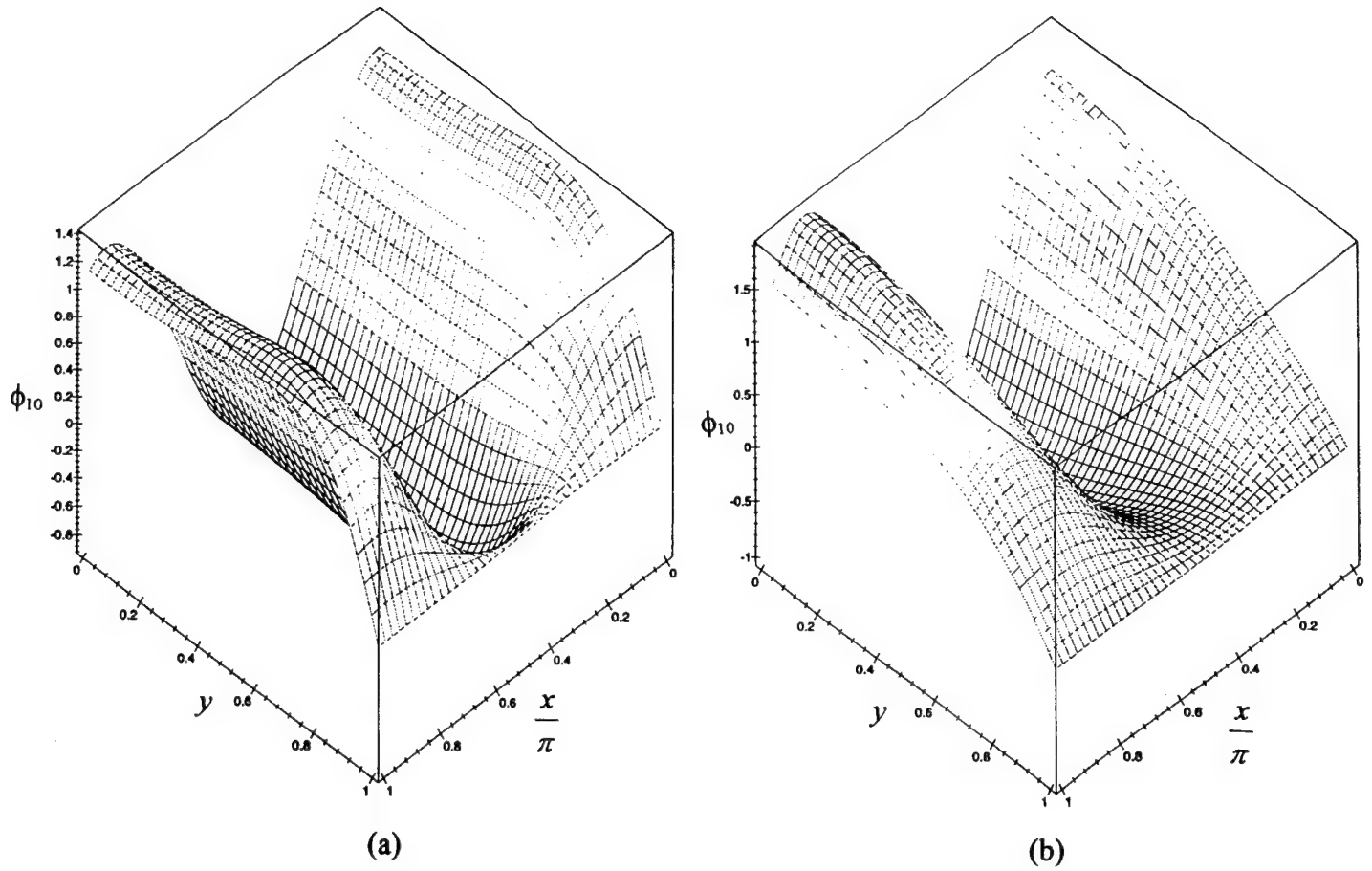

Figure 4.9 Time-Averaged Temperature Distribution, $\phi_{10}(x,y)$, for (a) $\eta_0\sqrt{\text{Pr}} = 5$ and (b) $\eta_0\sqrt{\text{Pr}} = 1.5$

combination of $\sin^2(mx)$ and $\cos^2(mx)$ terms. In Figure 4.10, the time-averaged temperature, $\phi_{10}(x,y)$, is shown for $x=0$, $x=\frac{\pi}{2}$ and $x=\pi$ and for $\eta_0\sqrt{\mathrm{Pr}}$ values of 1.5, 2, 3, and 5. The temperature, ϕ_{10}, vanishes at the wall ($y=1$), satisfying the no slip boundary condition; and its gradient, $\frac{\partial \phi_{10}}{\partial y}=0$ at the centerline ($y=0$), thereby satisfying the symmetry condition. From the $x=0$ curves, the variation in ϕ_{10} based on η_0 is clearly observed. For wide gaps or large η_0 values, the time-averaged temperature increases from zero at the wall to a maximum value fairly close to the wall and then decreases gradually, leveling off to a zero slope at the centerline. Thus, for wide gaps most of the temperature variation occurs near the wall. As the gap size becomes smaller or η_0 decreases, the magnitude of the time-averaged temperature gradient decreases, and the temperature variation is spread more and more evenly across the channel width. Further discussion of the affect on the time-averaged temperature gradient of varying the gap width is presented in the next section on the recovery factor. The time-averaged temperature distribution, $\phi_{10}(x,y)$, is not symmetric in x. This is illustrated by the fact that the plots for $x=\pi$ do not overlap with the curves for $x=0$.

D. THE RECOVERY FACTOR

More important than the results for the time-averaged temperature distribution, ϕ_{10}, presented above, it is the gradient of this temperature at the wall which allows key deductions to be made about the time-averaged heat transfer effects in this problem. In order to interpret these heat transfer results in a more conventional manner, they are

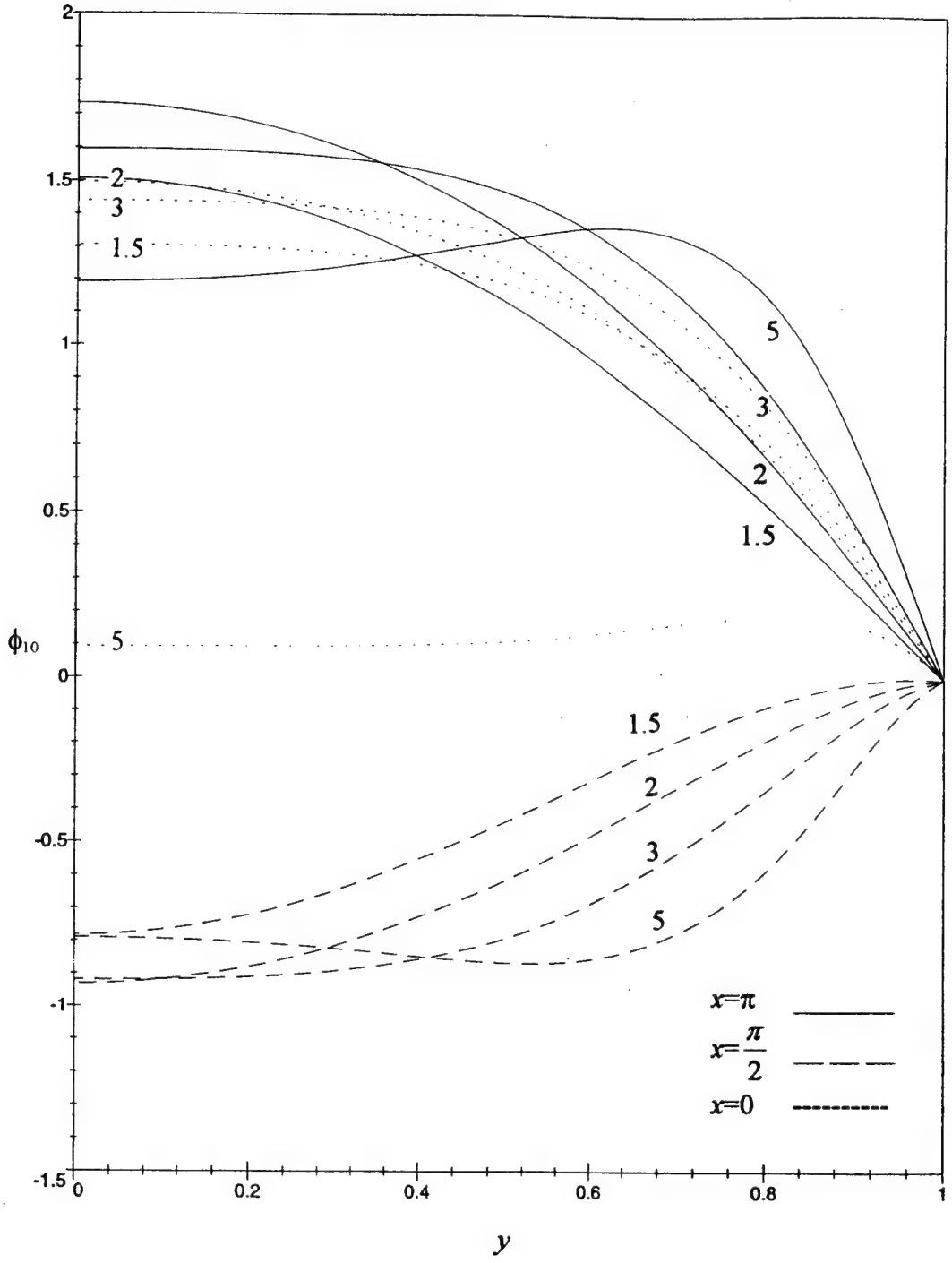

Figure 4.10 Time-Averaged Temperature Distribution, $\phi_{10}(x,y)$, for x=0, $x=\frac{\pi}{2}$ and x=π, and for $\eta_0\sqrt{\mathrm{Pr}}$ = 1.5, 2, 3, and 5

presented in terms of a suitably defined recovery factor. The recovery factor, r, is the ratio of recovered thermal energy at an adiabatic surface to the fluid's kinetic energy as discussed in Chapter II. The form of "r" utilized in this research conforms to convention and is given by

$$r = \frac{c_p (T_{aw} - T_m)}{\frac{V_0^2}{2}} \tag{4.7}$$

T_m is the fixed temperature of the upper plate. T_{aw} is the adiabatic wall temperature and it is equal to the value of T^* at y^*=-y_0 when the wall there is adiabatic. The adiabatic condition is that the temperature gradient, $\frac{\partial T^*}{\partial y^*} = 0$ at the wall in question, y^*=-y_0. In the present problem, T_{aw} would correspond to the time-averaged temperature achieved by a wall if it were made adiabatic. Let the corresponding dimensionless temperature for this adiabatic wall be denoted in general as ψ. Then it is the corresponding time-averaged temperature, ψ_{10}, at the adiabatic wall that is of interest here. Expressing the recovery factor and the adiabatic conditions in terms of the dimensionless parameters yields:

$$\begin{aligned}
&\frac{\partial \psi_{10}}{\partial y} \Delta T_{ref} = 0 \qquad \text{at} \quad y = -1, \\
&T_{aw} = \psi_{10} \Delta T_{ref} + T_m \quad \text{at} \quad y = -1, \\
&r = \frac{c_p (\psi_{10} \Delta T_{ref} + T_m - T_m)}{\frac{V_0^2}{2}} = \frac{\psi_{10} \Delta T_{ref}}{\frac{V_0^2}{2c_p}} = \psi_{10}, \\
&\text{or} \qquad r = \psi_{10} (y = -1)
\end{aligned} \tag{4.8}$$

where ψ_{10} is the dimensionless time-averaged temperature obtained in the adiabatic wall case.

In order to find "r" in this manner, however, it is necessary to additionally solve for the temperature distribution, ψ_{10}, in the adiabatic wall case. To avoid this extra time-consuming step, a relationship will be proven between the value of the time-averaged temperature, ψ_{10}, at an adiabatic wall and the value of the time-averaged temperature gradient, $\frac{\partial \phi_{10}}{\partial y}$, at the wall in the fixed temperature case that is the subject of this research. The two distributions appear to have approximate shapes as given in Figure 4.11.

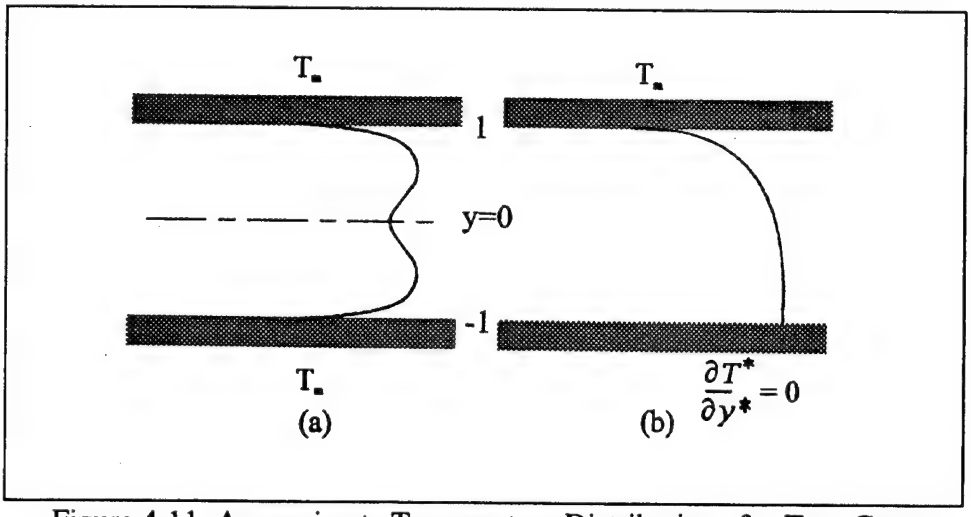

Figure 4.11 Approximate Temperature Distributions for Two Cases: (a) Fixed Wall Temperature and (b) Adiabatic Wall Temperature

$$\phi_{10} = \frac{T^* - T_m}{\frac{V_0^2}{2c_p}}$$

Boundary Conditions:

$\phi_{10} = 0$ at $y = \pm 1$

$\frac{\partial \phi_{10}}{\partial y} = 0$ at $y = 0$

$$\psi_{10} = \frac{T^* - T_m}{\frac{V_0^2}{2c_p}}$$

Boundary Conditions:

$\psi_{10} = 0$ at $y = 1$

$\frac{\partial \psi_{10}}{\partial y} = 0$ at $y = -1$

The recovery factor has already been shown in Equation 4.8 to be equal to $\psi_{10}(y=-1)$. It will now be proven that $\psi_{10}(y=-1) = 2\frac{\partial \phi_{10}}{\partial y}(y=-1)$. From the nature of the partial differential equation for ϕ_{10} in Equation 4.6, it is known that the y dependence of ϕ_{10} can be expressed as

$$\phi_{10}(y) = f(y) + C_1 y + C_2 \tag{4.9}$$

where from the nature of the forcing function in Equation 4.6, it can be shown that $f(y)$ is an even function. Now, applying the appropriate boundary conditions at the walls for the present problem yields

$$\begin{aligned} &\phi_{10}(1) = 0 = f(1) + C_1 + C_2 \quad \text{and} \\ &\phi_{10}(-1) = 0 = f(-1) - C_1 + C_2 \end{aligned} \tag{4.10}$$

Since $f(y)$ is an even function, $f(1)=f(-1)$, and the constants of integration are determined to be $C_1 = 0$ and $C_2 = -f(1)$. Thus, the resulting expressions for ϕ_{10} and $\frac{\partial \phi_{10}}{\partial y}$ are

$$\phi_{10}(y) = f(y) - f(1) \tag{4.11}$$

$$\frac{\partial \phi_{10}}{\partial y} = f'(y) \tag{4.12}$$

Similarly, for the adiabatic wall problem, the time-averaged temperature has the same governing equation since the primary leading order variables are the same. Then, ψ_{10} is expressed as the same function of y but with different constants of integration as follows:

$$\psi_{10}(y) = f(y) + D_1 y + D_2 \tag{4.13}$$

Applying the appropriate boundary conditions for this case, which are $\psi_{10}=0$ at $y=1$ and $\frac{\partial \psi_{10}}{\partial y}=0$ at $y=-1$, yields

$$\begin{aligned} \psi_{10}(1) &= 0 = f(1) + D_1 + D_2 \quad \text{and} \\ \frac{\partial \psi_{10}}{\partial y}(1) &= 0 = f'(1) + D_1 \end{aligned} \tag{4.14}$$

Thus, the constants are found to be $D_1 = -f'(-1)$ and $D_2 = f'(-1) - f(1)$, and the resulting function is found to be

$$\psi_{10}(y) = f(y) - f'(-1)y + f'(-1) - f(1) \tag{4.15}$$

Evaluating the adiabatic wall temperature, ψ_{10} at $y=-1$, yields

$$\psi_{10}(-1) = f(-1) + f'(-1) + f'(-1) - f(1) \tag{4.16}$$

Again, noting that $f(y)$ is an even function and using the properties of even functions, the previous equation is reduced to

$$\psi_{10}(-1) = 2f'(-1) \tag{4.17}$$

Also, from Equation 4.12, it is seen that $\frac{\partial \phi_{10}}{\partial y}(y=-1) = f'(-1)$. Therefore,

$$\psi_{10}(-1) = r = 2\frac{\partial \phi_{10}}{\partial y}(y=-1) \tag{4.18}$$

This proof allows "r" to be defined and calculated in terms of the temperature distribution, ϕ_{10}, which has been determined in the present problem without having to redo all of the work necessary to solve the adiabatic wall case. The gradient, $\frac{\partial \phi_{10}}{\partial y}$, is easily obtained and evaluated at the wall and then doubled. Since $f(y)$ is an even function, $f'(y)$ is an odd function; therefore, it is known that $f'(-1) = -f'(1)$. The domain of

analysis is $0 \le y \le 1$; therefore, for convenience, the recovery factor calculated in this research is determined by

$$r = -2\frac{\partial \phi_{10}}{\partial y}(y = 1) \tag{4.19}$$

The resulting values of "*r*" may be positive or negative. Positive values of "*r*" correspond with the physical situation of the wall being heated by the fluid. This phenomenon of the walls being heated by viscous dissipation is observed in high speed mean flows such as in the example cases presented in Chapter II. Negative values of the recovery factor indicate that the direction of heat flow is away from the wall as shown in Equation 4.19. In other words, the wall is actually being cooled by the fluid in those instances. This cooling potential is a very interesting attribute of high speed oscillatory flows, and it is this phenomenon which is the underlying principle that makes thermoacoustic refrigeration possible. Thermoacoustic heating and cooling effects caused by thermoacoustic streaming in a resonance tube were predicted theoretically and then validated experimentally by Merkli and Thomann (1975). A subsequent review of the topic was provided by Rott (1980). Experimental results were also obtained by Wheatley, et al. (1983) which verified the existence of this cooling effect in a stack of plates placed in an acoustically resonant tube.

The recovery factor, *r*, is calculated using Equation 4.19 and then plotted for each trial run for this problem. The results are illustrated in Figure 4.12 for one half of a wavelength, $0 \le x \le \pi$, and for $\eta_0\sqrt{\mathrm{Pr}}$ =1.5, 2, 3, and 5. For each gap width examined, the recovery factor takes on both positive and negative values which corresponds to

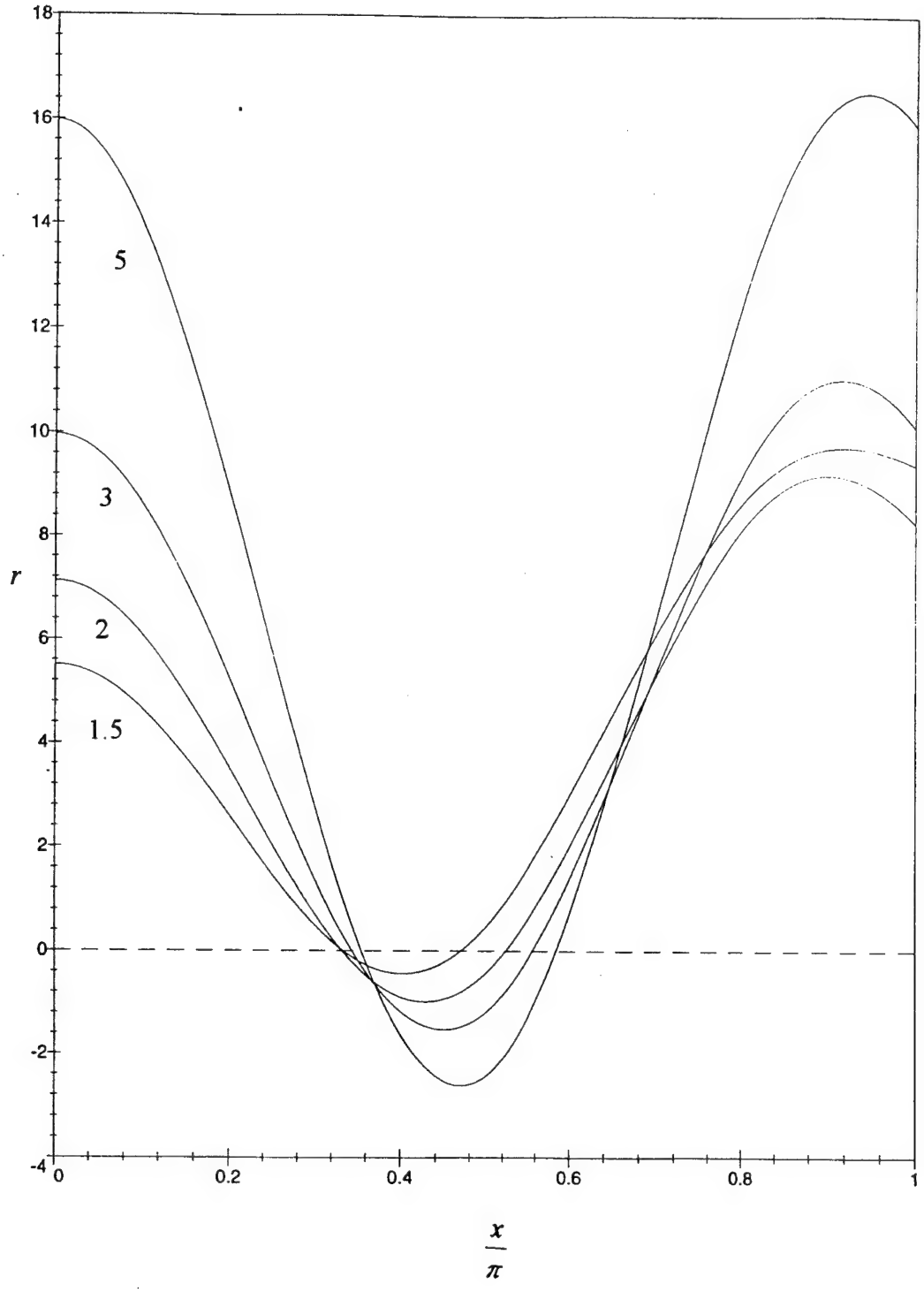

Figure 4.12 Recovery Factor, r, for $\eta_0\sqrt{\mathrm{Pr}}$ = 1.5, 2, 3, and 5

heating and cooling of the channel wall respectively. In general, at x=0, the recovery factor is a positive local maximum. As x increases, "r" decreases for each gap width until it reaches a minimum value which is negative. The recovery factor then increases as x increases until it reaches its maximum positive value before again beginning to decrease.

As observed in Figure 4.12, the recovery factor is generally higher in magnitude for all x values plotted and the curve is steeper (i.e. the gradients are higher in magnitude) for a wide gap than for a narrow gap. The fact that the "r" values are higher for wide gaps than for narrow gaps corresponds with the higher time-averaged temperature gradients observed near the wall (y=1) for wide gaps in Figure 4.10. According to Fourier's law as well as the meaning of the recovery factor as described earlier, these observations would imply greater heat fluxes for greater gap widths. This apparent implication does not agree, however, with what has been experimentally observed. Therefore, in order to better understand physically what "r" is measuring in this model problem of oscillatory flow, the equation for the recovery factor utilized in this work, Equation 4.19, is expanded by substituting back into it its dimensional quantities. From Equation 4.19, the recovery factor is proportional to the dimensionless time-averaged temperature gradient as follows:

$$r \propto \frac{\partial \phi_{10}}{\partial y} \tag{4.20}$$

Using the appropriate scaling relations involving ϕ_{10} and y from Equations 3.4 and 3.5, the relationship in Equation 4.20 becomes

$$r \propto \frac{y_0}{\left(\frac{V_0^2}{2c_p}\right)} \frac{\partial T_{10}^*}{\partial y^*} \tag{4.21}$$

Manipulating the expression in Equation 4.21 in order to relate the recovery factor to the physical parameters which are more appropriate for this oscillatory flow problem produces

$$r \propto \frac{\left(\frac{y_0}{\delta_\alpha}\right)\delta_\alpha}{\left(\frac{V_0^2}{c^2}\right)\left(\frac{c^2}{2c_p}\right)} \frac{\partial T_{10}^*}{\partial y^*} \tag{4.22}$$

where $\frac{y_0}{\delta_\alpha} = \eta_0\sqrt{\mathrm{Pr}}$ is again the gap width parameter utilized in this work. Substituting the relations, $M = \frac{V_0}{c}$ and $c^2 = \gamma R T_m$, into Equation 4.22, the expression for the recovery factor becomes

$$r \propto \frac{\left(\frac{y_0}{\delta_\alpha}\right)}{M^2\left(\frac{\gamma-1}{2}\right)} \frac{\partial\left(T_{10}^*/T_m\right)}{\partial\left(y^*/\delta_\alpha\right)} = \frac{\eta_0\sqrt{\mathrm{Pr}}}{M^2\left(\frac{\gamma-1}{2}\right)} \frac{\partial\left(T_{10}^*/T_m\right)}{\partial\left(y^*/\delta_\alpha\right)} \tag{4.23}$$

From Equation 4.23, the apparent contradiction to physics observed in Figure 4.12 is explained. It is clear from Equation 4.23 that for increasing values of $\eta_0\sqrt{\mathrm{Pr}}$, an increase in the magnitude of "*r*" does not automatically imply an increase in the time-averaged temperature gradient on the right hand side (RHS). In order to distinguish clearly the effect on the time-averaged temperature gradient as the gap width (or $\eta_0\sqrt{\mathrm{Pr}}$) changes, the recovery factor, *r*, must be scaled by $\eta_0\sqrt{\mathrm{Pr}}$ as follows:

$$\frac{r}{\eta_0\sqrt{\mathrm{Pr}}} \propto \frac{1}{M^2(\frac{\gamma-1}{2})}\frac{\partial(T_{t0}^*/T_m)}{\partial(y^*/\delta_\alpha)} \tag{4.24}$$

Therefore, for a given Mach number, M, and for a particular gas (i.e. γ fixed), the quantity, $\frac{r}{\eta_0\sqrt{\mathrm{Pr}}}$, in Equation 4.24, carries the physical information about how the time-averaged temperature gradient (and thus the heat flux) varies with different gap widths (or values of $\eta_0\sqrt{\mathrm{Pr}}$).

The recovery factor, scaled by $\eta_0\sqrt{\mathrm{Pr}}$, is plotted in Figure 4.13 for $\eta_0\sqrt{\mathrm{Pr}}$ = 1.5, 2, 3, and 5 and illustrates the true heating and cooling effects at the wall (y=1). For a wide gap as compared to a narrow gap, the "scaled recovery factor" ($\frac{r}{\eta_0\sqrt{\mathrm{Pr}}}$) is lower in magnitude when x=0 and remains lower until approximately x= 0.2π. At this point all of the curves cross so that the scaled recovery factor is slightly higher in magnitude for wide gaps until it crosses zero. During the initial cooling portion of the curve ($\frac{r}{\eta_0\sqrt{\mathrm{Pr}}}$<0), the wide gap magnitudes are lower again until the curves turn at their respective minima. Once the heating region is reached again ($\frac{r}{\eta_0\sqrt{\mathrm{Pr}}}$>0) for all of the curves, the scaled recovery factor is again lower in magnitude for wide gaps. The $\frac{r}{\eta_0\sqrt{\mathrm{Pr}}}$ curves are flatter (i.e. gradients are lower in magnitude) for wide gaps for generally all values of $\frac{r}{\eta_0\sqrt{\mathrm{Pr}}}$. Considering the portion of the curves where the scaled recovery factor is negative, the

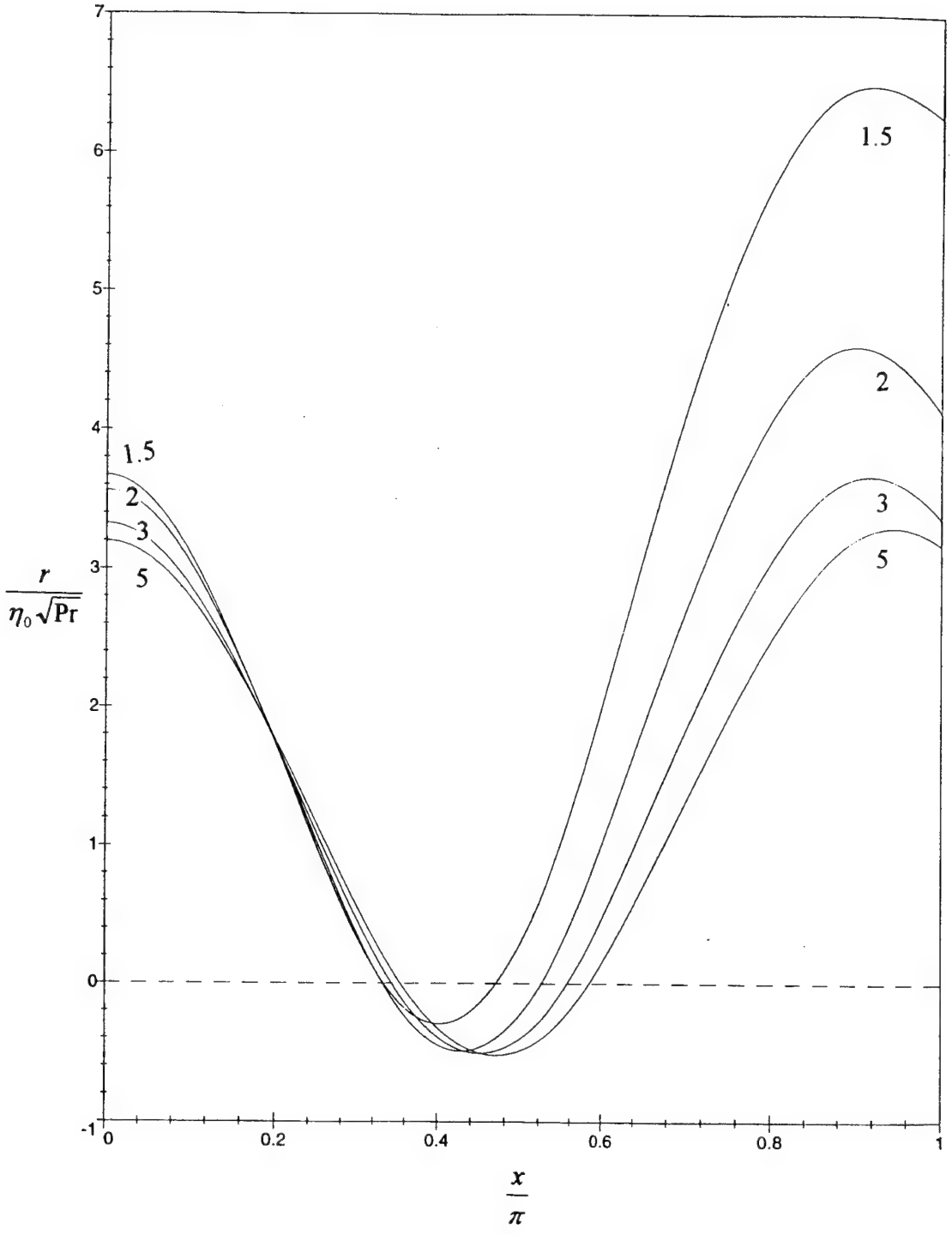

Figure 4.13 Recovery Factor Scaled to Show Heating and Cooling Effects, $\frac{r}{\eta_0\sqrt{\mathrm{Pr}}}$, for $\eta_0\sqrt{\mathrm{Pr}}$ = 1.5, 2, 3, and 5

following observations are noted. For $\eta_0\sqrt{\mathrm{Pr}}=5$, the zero crossings of the scaled recovery factor occur at approximately $x=0.36\pi$ and $x=0.58\pi$. Thus, the length of the x-interval for which $\frac{r}{\eta_0\sqrt{\mathrm{Pr}}}$ is negative is approximately 0.22π. As the gap width narrows or η_0 decreases, the average magnitude of the scaled recovery factor decreases and the magnitude of its gradient increases. This results in a shift of both zero crossings to lower x values as η_0 decreases as well as a shortening of the x-interval over which the scaled recovery factor is negative. For example, when $\eta_0\sqrt{\mathrm{Pr}}=1.5$, the zero crossings of the scaled recovery factor occur at approximately $x=0.33\pi$ and $x=0.46\pi$, resulting in an x-interval where the $\frac{r}{\eta_0\sqrt{\mathrm{Pr}}}$ value is negative of approximately 0.13π.

The higher magnitudes of the positive scaled recovery factor for narrower gaps translate into higher heat fluxes at the wall of the channel for those x locations. Just as in the previous discussion concerning the conventional recovery factor, r, for the x-intervals where the scaled recovery factor is positive, the channel wall is being heated by the fluid through viscous dissipation. For the x-interval where $\frac{r}{\eta_0\sqrt{\mathrm{Pr}}}$ is negative, the channel wall is actually being cooled by the oscillating fluid. The gradient of $\frac{r}{\eta_0\sqrt{\mathrm{Pr}}}$ is also important because it determines the heat pumping capacity available. More specifically, for the same magnitude of $\frac{r}{\eta_0\sqrt{\mathrm{Pr}}}$ (or cooling effect), a higher gradient equates to more heat pumping capacity available for the same length of plates.

This cooling effect, produced in zero-mean oscillatory flows, is utilized in thermoacoustic refrigeration applications. The stack of the thermoacoustic refrigerator is positioned in a tube where part of the stack is in a region of x values where the scaled recovery factor is positive, and the remaining portion of the stack is in a region where $\frac{r}{\eta_0\sqrt{\mathrm{Pr}}}$ is negative. The end where cooling occurs (negative $\frac{r}{\eta_0\sqrt{\mathrm{Pr}}}$ values) is where the refrigerating effect is produced. The heat generated at the other end of the stack (where the scaled recovery factor is positive) is removed via a heat sink. The stack region of a typical thermoacoustic refrigerator is very short compared to the wavelength of the acoustic wave producing the oscillatory flow; therefore, an analysis of the scaled recovery factor in the region of x where $\frac{r}{\eta_0\sqrt{\mathrm{Pr}}}$ just becomes negative is important for this application. Comparing both the magnitudes of $\frac{r}{\eta_0\sqrt{\mathrm{Pr}}}$ and the gradients in the region of x from approximately 0.33π to approximately 0.4π in Figure 4.13, it is observed that the highest magnitude and gradient of the scaled recovery factor occur for the case where $\eta_0\sqrt{\mathrm{Pr}}=2$. Therefore, for a stack place with its cooling end in that x region, the heat flux away from the wall and the heat pumping capacity are both greater for a gap width corresponding to $\eta_0\sqrt{\mathrm{Pr}}=2$ than for any of the other gap widths examined.

V. CONCLUSION

This work involved finding the analytical solution to a fundamental problem in order to study the time-averaged heat transfer effects induced by high speed zero-mean internal oscillatory flows. The governing equations of continuity, momentum, energy, and state were established for the model problem which consisted of an ideal-gas host fluid between two parallel plates excited into a zero-mean oscillatory flow by a high-intensity standing acoustic wave.

Introducing the proper scaling relations, the governing equations were transformed into dimensionless equations; then, order of magnitude analyses were conducted to simplify the resulting equations. Employing perturbation solution methods with the Mach number, M, used as a perturbation parameter, the equations were expanded and separated based on the orders of M. The most significant order equations were then analytically solved using complex variable methods for the unknown velocity, density, temperature, and pressure terms. The final aim was to determine the time-averaged temperature distribution for various gap widths in order to analyze the heat transfer effects induced by the zero-mean oscillatory flow.

The analysis was completed using air as the host fluid for gap widths corresponding to various $\eta_0\sqrt{\mathrm{Pr}}$ values up to $\eta_0\sqrt{\mathrm{Pr}}=5$, which was determined to be the lower limit for consideration as a "wide gap". The leading order primary variables were presented graphically and discussed in detail in Chapter IV along with the time-averaged temperature and corresponding recovery factors. According to the interpretation of these

results, using air as the host fluid, the most suitable choice of gap width in terms of the cooling effects applicable to thermoacoustic refrigeration corresponded to a value of $\eta_0\sqrt{Pr}=2$.

This was a fundamental study, hoped to be a foundation upon which to be built, in the area of recovery factors in zero-mean internal oscillatory flows. Further work is suggested such as determining the most suitable gas to be used as a host fluid (i.e. to maximize the cooling effects produced). Also, model problems involving different geometries (such as cylindrical or annulus) should be solved in a similar manner to the present parallel plate problem. A potential source of difficulty in solving problems using more complicated coordinate systems is the ability (or possible inability) of MAPLE to solve the final equation for the time-averaged temperature term.

LIST OF REFERENCES

Blachman, N.R., and Mossinghoff, M.J., *MAPLE V Quick Reference*, Brooks/Cole Publishing Company, 1994.

Burmeister, L.C., *Convective Heat Transfer*, John Wiley & Sons, Inc., 1983.

Merkli, P., and Thomann, H., Thermoacoustic effects in a resonance tube, *J. Fluid Mech.*, **70**, 161-177, (1975).

Rott, N., Thermoacoustics, *Adv. Appl. Mech.*, **20**, 135-175, (1980).

Schlichting, H., *Boundary-Layer Theory*, Seventh Edition, McGraw-Hill, Inc., 1979.

Wheatley, J., Hofler, T., Swift, G.W., and Migliori, A., An intrinsically irreversible thermoacoustic heat engine, *J. Acoust. Soc. Am.*, **74** (1), 153-170, (1983).

INITIAL DISTRIBUTION LIST

1. Defense Technical Information Center.....2
   8725 John J. Kingman Rd., STE 0944
   Fort Belvoir, Virginia 22060-6218

2. Library, Code 13.....2
   Naval Postgraduate School
   Monterey, California 93943-5101

3. Ashok Gopinath.....1
   Department of Mechanical Engineering, Code ME/Gk
   Naval Postgraduate School
   Monterey, California 93943

4. Oscar Biblarz.....1
   Department of Aeronautical and Astronautical Engineering, Code AA/Bi
   Naval Postgraduate School
   Monterey, California 93943

5. M. D. Kelleher, Chairman.....1
   Department of Mechanical Engineering, Code ME/Kk
   Naval Postgraduate School
   Monterey, California 93943

6. D. J. Collins, Chairman.....1
   Department of Aeronautical and Astronautical Engineering, Code AA/Co
   Naval Postgraduate School
   Monterey, California 93943

7. Nicole Lynn Tait.....1
   c/o Vicki Maisonneuve
   9703 48th Place
   College Park, Maryland 20740